Journal of Building Engineering 114 (2025) 114118

Contents lists available at ScienceDirect

Journal of Building Engineering

journal homepage: www.elsevier.com/locate/jobe

Experimental investigations on the bond performance of reinforced concrete beam with lap splices after fire exposure

Arunita Das [a,*], Josipa Bošnjak [b], Akanshu Sharma [c]

[a] Institute of Construction Materials, University of Stuttgart, Stuttgart, Germany
[b] Material Testing Institute, University of Stuttgart, Stuttgart, Germany
[c] Lyles School of Civil Engineering, Purdue University, West Lafayette, IN, USA

ARTICLE INFO

Keywords:
Lap splices
ISO 834 fire
Concrete splitting
Flexural strength
Residual capacity
Steel-to-concrete bond

ABSTRACT

The manufacturing and transportation limitations necessitate splicing of the reinforcing bars for the construction of most reinforced concrete (RC) structures. Lap splices present a particular challenge in case of a fire incident, as the local damage in the concrete cover region can significantly affect the structural performance. There are multiple studies on post-fire bond behaviour, however, only a few studies focused on its implications at the structural level. In order to bridge this gap, the research reported herein focused on the post-fire performance of lap splices. RC beams without and with tension lap splices were tested in four-point bending, whereby different lap lengths were considered (20–50 times the bar diameter). The beams were exposed to a standard ISO 834 fire for 60 min and bending tests were performed in residual state thereafter. To avoid possible explosive spalling, 1 kg/m^3 of polypropylene fibers were added to the concrete mix. It is observed that fire has a strong impact on the beams with lap splices whereas beams with continuous reinforcement almost maintain their original flexural capacity in post-fire state. The results are compared with the results obtained in the previous studies by the authors using beam-end specimens. The design concept proposed forms the basis of the new provisions in fib Model Code 2020 for the design of lap splices under fire.

1. Introduction

During the service life of a reinforced concrete structure, fire is one of the most severe events which it may encounter. In case of such a destructive event, despite concrete being incombustible in nature and providing excellent thermal resistance, the performance of a RC structure may deteriorate significantly. Not only the material properties of concrete and steel degrade due to fire but also the integrity of bond between steel and concrete, which is one of the governing aspects of structural behaviour, may be adversely affected.

For the ease of transportation and handling in the construction sites, the reinforcing bars are often cut after a certain length and therefore they need to be spliced when used in a structure. To maintain the structural integrity and functionality, it is essential to have a proper transmission of the stresses between the spliced rebars. In practice, though there are many splicing methods available, such as lap splices, mechanical couplers, welded splices etc., lap splice is the most predominately and widely used splice method in reinforcing bars due to its simplicity in operation and cost-effectiveness in connecting the rebars. Moreover, from the practicality point of view in construction, i.e. construction projects often face adjustments and modifications, and lap splicing provides the flexibility needed to

* Corresponding author.
E-mail address: arunitadas2008@gmail.com (A. Das).

https://doi.org/10.1016/j.jobe.2025.114118
Received 4 May 2025; Received in revised form 28 August 2025; Accepted 17 September 2025
Available online 25 September 2025

extend or connect rebars as the construction progresses, accommodating changes in design or structure requirements. In the case of lap splices, the lap length must be sufficient to assure the safe transfer of the tensile stresses from 1 bar to another to maintain the structural integrity and performance. The tensile stress in the bar is maximum at the point where the splice begins and gradually decreases to zero towards the free end. This gradient in axial stresses results in the development of relatively high bond stresses within the splice region.

For a well-designed tension splice steel yielding of the spliced bars should be achieved prior to bond splitting failure of the splice. The splice lengths required by the design codes and standards are expected to develop the bars ensuring a ductile failure mechanism. However, these provisions are valid only for structural members under ambient conditions. When a RC beam with a lap splice is exposed to fire, due to the thermal damage and the degradation of material properties, bond splitting failure of the splice may govern the failure mechanism, especially in post-fire scenario. Consequently, it may happen that though the length of the lap splice is sufficient for achieving a ductile failure mode in ambient condition, in the residual (post-fire) state the same length of lap splice can be insufficient to ensure steel yielding prior to bond splitting failure.

In the past, the authors have carried out an extensive investigation on the post-fire bond performance between steel and concrete using beam-end specimen considering real fire scenarios [1–5]. The influence of several major parameters impacting the residual bond performances such as concrete cover, confinement, position of rebars, diameter of rebar, bonded length, duration of fire, different heating scenarios, consideration of twin rebars was investigated. It was found that the fire has a strong influence on the residual bond performance irrespective of the other parameters. The consideration of beam-end specimen over standard pull-out specimen was found to have an important insight on the realistic simulation of the structural bond behaviour under ambient and post-fire conditions.

Though the beam-end specimens utilized by authors were useful to investigate the local bond degradation, these could not replicate the condition in a lap splice completely, especially the bending effect present in flexural members and non-uniform bond stress distribution along the long splice length. To characterize the influence of fire on the residual performance of lap splices under realistic conditions, in this work, tests have been carried out on beams with different splice lengths subjected to a standard ISO 834 fire for 60 min and tested under 4-point bending in residual state (after cooling down to room temperature). The beams were not subjected to any mechanical load during the exposure to fire. Since the primary objective of this study was to investigate the influence of fire on bond and lap splices, Polypropylene (PP) fibers were added to the mix to mitigate explosive spalling of concrete during fire. The quantity added (1 kg/m^3) of PP fibers is not expected to significantly impact the mechanical and physical properties of concrete at ambient conditions (Bosnjak et al., 2019 [6]).

Over the years, significant research on the capacity of beams with lap splice in ambient condition has been performed. However, the post-fire performance of beams with lap splices has received limited attention. Therefore, current design codes (EN 1992-1-2:2010 [7], ASTM E2748 - 12a [8], ACI 216.1-14 [9]) do not consider the bond degradation under fire while calculating the structural performance of the beams under fire, either during fire or in post-fire conditions. The existing studies on residual performance of beams with spliced reinforcement after exposure to fire or elevated temperatures are summarized in the following.

Rehman et al. [10] performed investigations on the flexural bond behaviour of reinforced concrete beams with different development length at the mid-span exposed to elevated temperature. Beams with cross sections of 80 mm × 120 mm and a length of 900 mm were used in the study. A single rebar sliced at the mid-section of the beam was considered. The study analysed different lap lengths (200 mm, 250 mm and 300 mm) and rebar diameters (8 mm, 10 mm and 12 mm). A single heating-cooling cycle of elevated temperature ranging from a minimum temperature of 200 °C to a maximum temperature of 800 °C at an interval of 200 °C with a slow heating rate of 5 °C/min for a heating duration of 3 h was considered in the study. It was concluded that the residual bond strength and stiffness decrease with the increase of temperature, and the cracks propagate in the horizontal directions and concentrate mostly in the lap splice region.

Irheem et al. [11] performed experimental investigations on the residual capacity of RC beams considering a lap splice length of 600 mm and 12 mm rebars (lap splice length of 50d_s, d_s - rebar diameter) after exposure to fire. Beams with a cross section of 150 mm × 300 mm and a length of 3000 mm were considered in the study. For the fire exposure of the beams standard fire curve (ISO 834-1) was used, but only up to the temperature range of 650 °C and 800 °C for three different exposure durations (1, 2, and 3 h). Only the bottom surface of the beams was exposed to fire. Two different clear covers (20 mm and 30 mm) were investigated. Though it was outlined that the fire exposure changes the failure mode from ductile flexural to splitting in the majority of the beam specimens, fire caused only a moderate degradation of the residual ultimate load capacity of the beams. Post heating load capacity was reported as 65 %–95 % of the capacity of the specimens in the ambient condition (unheated). Though this research lay a foundation by demonstrating the effect of the fire on the residual capacity of beams, there is still a need to understand the realistic behaviour, as in case of real fire the maximum temperature typically rises to much higher than 850 °C and all the surfaces of the beams may be exposed to fire.

A similar investigation was conducted by Hossain-Zada [12]. The beams with lap splices were exposed to elevated temperature (T_{max} = 600 °C, heating rate approx. 6 °C/min up to 300 °C and approx. 0.7 °C/min thereafter) and the residual capacity of the beams was studied by conducting four-point bending tests in residual state. Splice length was 150 mm, corresponding to 15d_s. Similar to Irhem et al. [11], it was concluded that the exposure to elevated temperature changes the failure mode of beams with lap splice from ductile flexural to splitting. At the second stage of the investigation the use of hybrid fibers (0.75 % vol. steel fibers and 0.15 % vol. polypropylene fibers) on improving the flexural performance of the heat exposed beams with lap splice was studied. It was found that adding hybrid fibers can increase the bending capacity for beams with lap splices and even prevent brittle splitting failure observed upon heating. While this study provides an insight in the change of failure mode of beams with splices after high temperature exposure, it does not fully capture the impact of real fire as a maximum exposure temperature of only 600 °C and a relatively slow heating rate were considered for the study.

Sharma et al. [13] investigated the post-fire behaviour of beams without and with lap splices in the tension zone considering a 16 mm rebar and a lap splice length of 300 mm (19d_s) in the mid-span. Rectangular reinforced concrete beams with a cross section of 200

mm × 300 mm and a length of 3200 mm were used for the investigations. Standard fire scenario acc. to ISO 834-1 was considered, whereby the beams were exposed to 60- and 90-min fire. Four-point bending tests were performed on the fire damaged beams in residual state. The specimens were designed such that in ambient condition the steel yielding failure mode of the beams with continuous rebars changed to bond splitting failure mode for the beams with lap splice. In the case of residual loading after fire exposure, all beams with continuous reinforcement exhibited steel yielding whereas the beams with spliced reinforcement experienced bond splitting. The reduction in the post-fire flexural capacity of beams with continuous reinforcement was found to be rather insignificant, with maximum degradation of flexural capacity of 10 % after 90 min of fire. On the other hand, the beams with lap splice exhibited a severe degradation of the capacity, as the 60 min and 90 min of fire exposure duration led to a reduction in the residual capacity of 54 % and 66 % respectively, which was attributed to aggravated concrete damage during heating and cooling. Tonidis et al. [14] further continued the investigation by performing the numerical parametric study, which included the influence of different splice length on post-fire performance of the beams.

The abovementioned studies underlined the importance of considering structural performance of flexural elements after fire exposure, however, the studies have not covered all relevant aspects. Some studies assumed quite moderate heating or only one-sided exposure of the beam to fire, which is not necessarily representative of the real fire scenario. Furthermore, previous experimental studies involved investigations only for one lap splice length.

To extend the experimental database and to address the gap in the existing research regarding the realistic fire scenario and the effect of lap splice length, the work presented herewith aims to investigate the bond behaviour of reinforced concrete beams with lap splices under bending by focusing on both the ambient and post-fire conditions for a range of lap splice lengths. Furthermore, a model/design concept for the assessment of the post-fire bond strengths of existing lap splice/anchorages as well as for the design of new splices/anchorages considering required fire rating are proposed. The proposed design concept was included in the recently published *fib* Model Code 2020 [15].

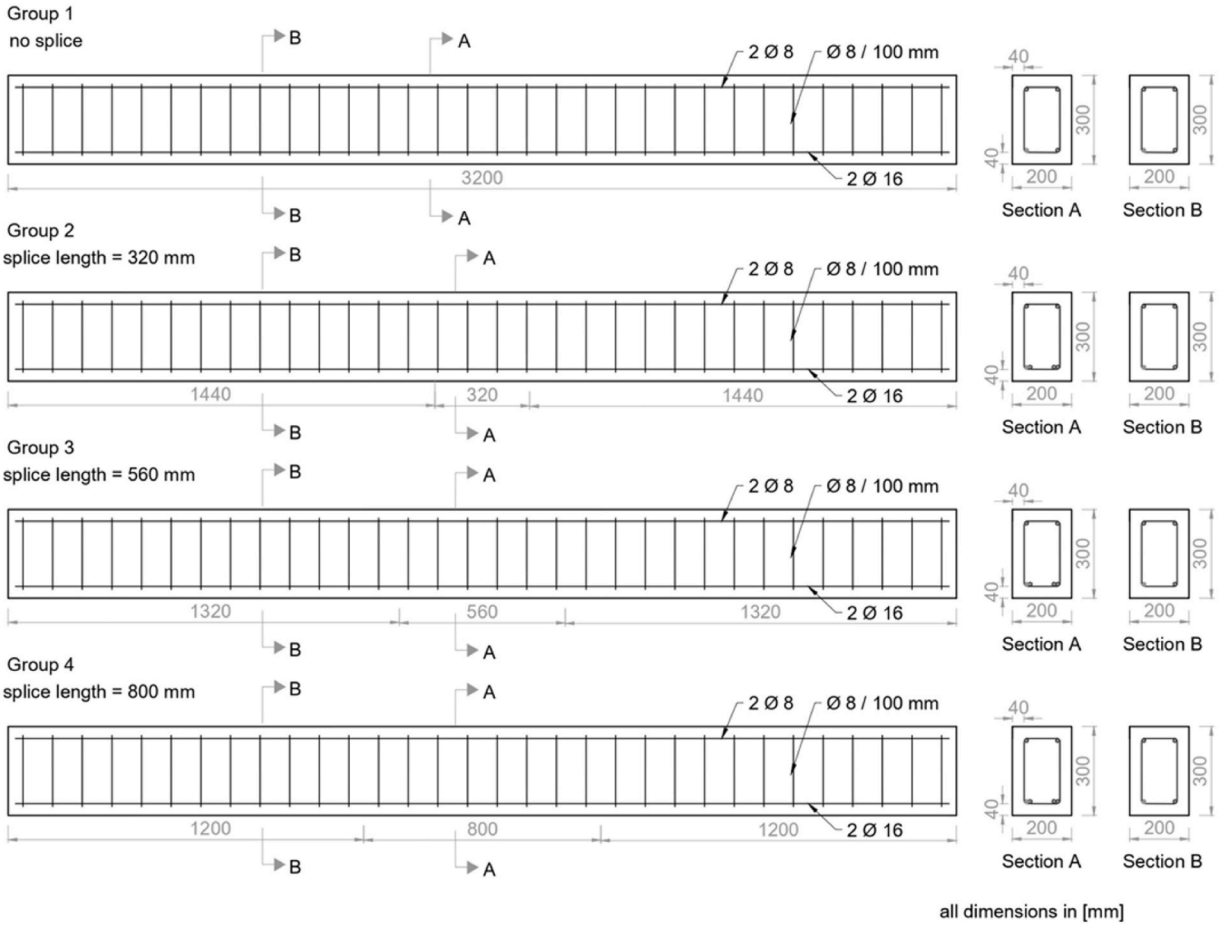

Fig. 1. Details of test specimens.

2. Experimental program

2.1. Test specimen

Eight reinforced concrete beams with rectangular cross-sections measuring 200 mm in width and 300 mm in height were tested. The beams featured a simply supported overall length of 3.2 m with a distance of 3 m between the supports. A total of four groups with 2 beams (one tested under ambient conditions and one tested after exposure to fire) per group were analysed (note that, Group 1 beams were tested by Sharma et al. [13], a detailed description can be found in 3.3.1). Fig. 1 presents the geometry, reinforcement configuration and dimensions of the tested beam groups. Each beam was reinforced with two tension rebars on the tension side and two continuous rebars in the compression zone, regardless of whether the beam had a tension lap splice or not. For beams with lap splices, four rebars were used in the splice region of the tension zone. The rebars in the tension zone were positioned with an axis distance of 48 mm from the bottom and side faces of the beam (providing 40 mm of clear cover). The tension zone was reinforced with two 16 mm deformed steel rebars, and compression zone were reinforced with two 8 mm deformed steel rebars. Shear reinforcement was provided by 8 mm diameter stirrups spaced at 100 mm c/c along the entire length of the beam. The reinforcement cages were secured using iron wires. Four different beam configurations were considered: i) group 1 - reference beams with continuous reinforcement, ii) group 2 - beams with lap splice length of 320 mm ($20d_s$), iii) group 3 - beams with lap splice length of 560 mm ($35d_s$) and iv) group 4 - beams with lap splice length of 800 mm ($50d_s$).

2.2. Specimen preparation

The test specimens were manufactured using concrete according to DIN EN 206 [16] from the precast concrete manufacturing facility at RAU in Ebhausen, Germany. The beams were cast in the plywood stiffened framework of desired dimensions with smooth surface to maintain the shape of the beam under the pressure of newly cast concrete. A clear concrete cover of 40 mm (see Fig. 1) was used on all the four sides of the beam. The mixing of concrete was performed in a rotating mixer. At a first step, the reinforcement cage was placed inside the form as depicted in Fig. 2. Before casting, thermocouples were fixed in the required positions.

The nominal strength concrete of 30 MPa at age of 28 days was targeted for the investigations. To minimize the scatter in terms of material properties, all the beams were prepared in a single batch of concrete. The maximum size of the coarse aggregate was 16 mm. Coarse aggregates were round river gravel. The details of the concrete mix are shown in Table 1. To achieve the desired workability, a plasticizer was also incorporated into the concrete mix. Polypropylene fibers (*Baumhüter REF 506*, diameter 15,6 μm, length 6 mm) were added to the mix to mitigate explosive spalling of concrete during fire. PP fibers do not significantly impact the mechanical and physical properties of concrete at ambient conditions, however, their role becomes important in case of a fire, as the permeability of concrete with PP fibers increases significantly when compared to the concrete without fibers. At elevated temperatures, PP fibers within the concrete matrix begin to melt. This melting occurs at temperatures significantly lower than those that would cause concrete to spall explosively. This facilitates the transport of water vapor, releases the water vapor pressure, and mitigates the explosive concrete spalling risk.

To measure and control the consistency of the fresh concrete, the slump test was conducted using the fresh concrete mix. The measured flow spread value of the slump test was 450 mm. As intended, in the investigated samples the slump grade of F3 was achieved.

To measure the temperature distribution inside the concrete layers during and after the fire exposure, K-type thermocouples (1 x NiCr-Ni, Type K, Form ES 30-T, Producer: E&S Metronics - Mess-und Regeltechnik GmbH, Werne) were placed at several locations of each beam. Fig. 2c presents the location of the thermocouples inside the beam. Three thermocouples were placed along the longitudinal tension rebar at three different locations namely at mid span and two quarter spans of the beam while other two thermocouples were placed on the stirrups at the midspan and the quarter span of the beam as shown in Fig. 2c.

The thermocouple nomenclature follows a systematic convention that allows easy identification of each sensor based on its location and the corresponding beam group. For example, TS_M_Gr2 designates a thermocouple (TS) attached to a stirrup at the mid-span (M) of a beam belonging to Group 2 (Gr2). Similarly, TL1/2_M_Gr2 refers to two thermocouples placed on the longitudinal rebars (TL)—one on each bar—also positioned at the mid-span of a Group 2 beam. The label TL2_Q_Gr1 indicates a thermocouple fixed to the second longitudinal rebar at the quarter-span (Q) of a Group 1 (Gr1) beam.

The thermocouples were hot junction insulated with Inconel 600 coating. The part of the thermocouple which was used inside the furnace was coated with mineral coating. A large length of approximately 4 m was considered for the inside use to provide sufficient protection against high temperatures attained in the furnace. The remaining part of the cable was insulated using PVC coating (length = 4 m), since this part was used only outside the furnace.

After mixing, the concrete mix was cast into forms. The fresh concrete was poured into the formwork in several layers and a standard needle vibrator was used for the compaction of concrete inside the framework. After the 24 h of casting of the beams, the sides of the mould were stripped and the initial curing of the test specimen, cubes and cylinders begun inside a closed warehouse. After curing the beams for up to approximately four weeks after casting, the beams were transported to the testing laboratory in the University of Stuttgart. All beams were equipped with four transport anchors to facilitate the crane transport of the specimens at the testing facility. The temperature of the testing laboratory was maintained at 20 °C–25 °C up to the day of the fire test at an age of approximately 3 months. This conditioning was required to prevent eventual explosive spalling of specimens during the fire tests.

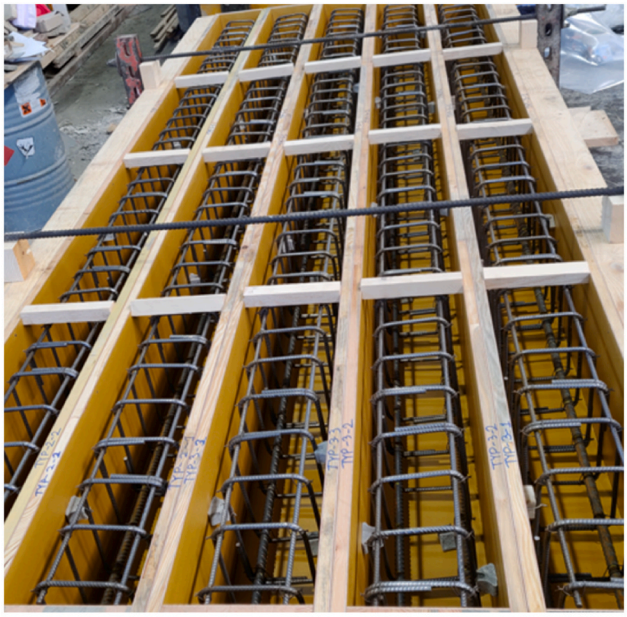

(a)

(b)

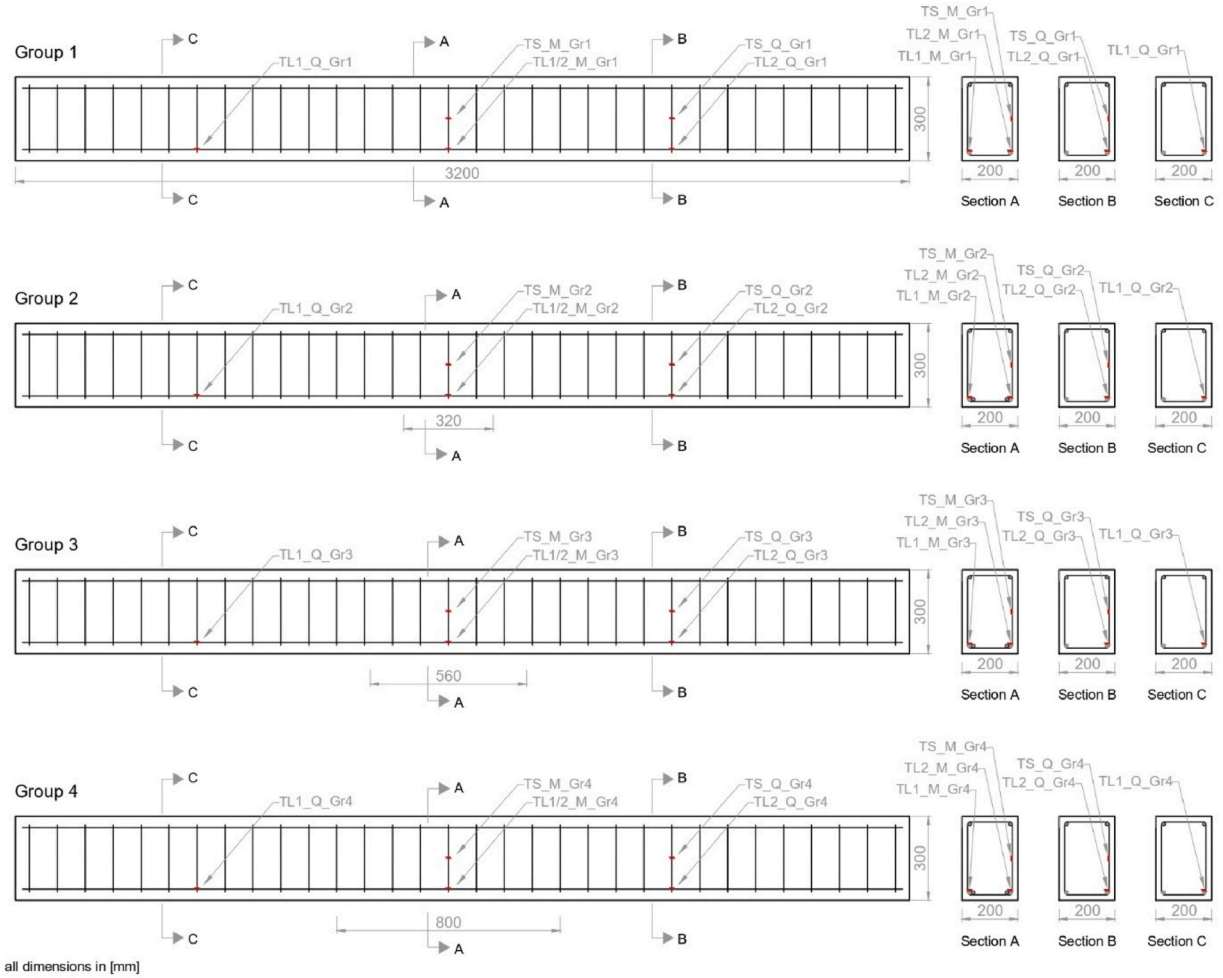

(c)

(caption on next page)

Fig. 2. The test specimens a) reinforcement cage before concreting, b) during the concreting and c) location for the embedded thermocouples along the cross-section.

2.3. Test program

Four groups of beams each containing two specimens were tested in this study. In each group, one beam (length 3200 mm, width 200 mm, height 300 mm) was kept as a reference specimen which was directly tested under four-point bending to failure, while the other beam was exposed to fire acc. to ISO 834 fire scenario [17] for 1 hour and subsequently tested under four-point bending. Following different beam configurations were considered: i) group 1 - reference beams with continuous reinforcement, ii) group 2 - beams with lap splice length of 320 mm ($20d_s$), iii) group 3 - beams with lap splice length of 560 mm ($35d_s$) and iv) group 4 - beams with lap splice length of 800 mm ($50d_s$). The splice length was chosen with respect to the code-specific requirements, i.e. the target was to have one splice length exactly as the codes require, one significantly shorter and one well above the code requirements. The 320 mm splice length ($20d_s$) is significantly shorter than the development length recommended by the code, while the 560 mm splice length ($35d_s$) is approximately equal to the code-specified development length. In contrast, the 800 mm splice length ($50d_s$) exceeds the recommended value, allowing for comparison of bond behaviour across splice lengths that are below, at, and above the code requirement.

All the lap splices in the tension zone were provided at mid-span. Therefore, except for the negligible effects due to the self-weight of the beams, there is a pure bending moment acting at the complete region of the lap splice length. In each case, a proportion of the 100 % lapped rebars in the tension zone were considered (i.e. both rebars were spliced at the same location).

Table 2 summarizes the considered beam test variables. A two-part notation system is used to represent the specimens of each group, where the identity code "B1 to B4" refers to the different groups of beams with or without lap splice. The identity code "R" refers to the reference beam (fire unexposed beam) and "F60" indicates a fire exposure duration of 60 min (It is important to note that, Group 1 beams were tested by Sharma et al. [13], a detailed description can be found in 3.3.1).

2.4. Material properties

The concrete mix was designed for target mean cube compressive strength at the time of testing (approximately 3 months) of 30 MPa. Cube specimens with dimensions 150 × 150 × 150 mm, cylinders with 150 mm diameter and 300 mm height were cast along with beams to determine the mechanical properties of concrete (compressive strength, Young's elasticity modulus and splitting tensile strength). The compression tests were carried out at the age of 7 days, 28 days and on the day of fire test (approximately 3 months after the casting) in accordance with DIN EN 12390-3 [18] while the splitting tensile were carried out at 28 days according to DIN EN 12390-6 [19]. Young's modulus was tested in accordance with EN 12390-13 [20]. All material properties are summarized in Table 3.

Standard BSt500 deformed bars as per DIN 488 (EN ISO 15630-1; EN ISO 15630-2 [21,22]) were utilized as the longitudinal reinforcement as well as the stirrups for the beams. The reinforcing steel was employed in its original condition i.e. with no surface preparation.

2.5. Test preparation

Experimental investigations on the residual flexural capacity of beams were carried out at the Materials Testing Institute,

Table 1
Concrete mix.

Target strength	Cement		Aggregates [kg/m^3]			Water		Plasticizer	PP fibres
MPa	type	kg/m^3	0–2	2–8	8–16	kg/m^3	w/c	wt.% cement	kg/m^3
30	CEM I 32,5 R	210	784	496	730	133	0.63	0.22	1.0

Notes: PP fibres = polypropylene fibres "Baumhüter" REF 506 (diameter 15.6 μm, length 6 mm).
Coarse aggregates were round river gravel.

Table 2
Test programme for the full-scale beams.

Beam	Lap splice length	Concrete cover	Fire exposure	Number of tested specimens	
				reference	post-fire
[−]	[mm]	[mm]	[−]	[−]	[−]
Group 1	No splice	40	three-sided	1 (B1_R)	1 (B1_F60)
Group 2	320	40	three-sided	1 (B2_R)	1 (B2_F60)
Group 3	560	40	three-sided	1 (B3_R)	1 (B3_F60)
Group 4	800	40	three-sided	1 (B4_R)	1 (B4_F60)

Table 3
Concrete properties.

Age	Cube compressive strength ($f_{c,\ cube}$)		Splitting strength ($f_{t,sp}$)		E-modulus (E)	
[days]	Measurements	Mean	Measurements	Mean	Measurements	Mean
	[N/mm^2]		[N/mm^2]		[GPa]	
7	16.70	16.70	–		–	–
28	23.30	23.30	–		–	–
81	28.24	27.96	2.45	2.477	27.8	27.87
	28.43		2.525		27.94	
	27.22		2.457			

University of Stuttgart. The work was performed in two steps: i) the beams were first placed in the furnace, subjected to fire for 60 min and left to cool down naturally to the ambient temperature, ii) the four-point bending test for determination of residual flexural capacity was carried out.

2.5.1. Fire test

A large furnace (length 8 m x width 2.4 m x height 2.5 m) with the capacity of accommodating all the beams was used for the fire test. A total of twelve burners, six on the either side of the wall enable the thermal exposure of the standard time-temperature curve (ISO 834 [17]) inside the furnace. The furnace internal environment was monitored with twelve sheath thermocouples, placed through the furnace roof. The locations of the temperature thermocouples (S1 to S6 and W1 to W6) are illustrated in Fig. 3a. The beams were positioned on the furnace roof, keeping a space of minimum 0.6 m between them. The design of slab was such as to allow the heat exposure to three sides of the beam which includes bottom surface and two flank surfaces. The length of the beam exposed to the heat on all three sides was 2410 mm. The top surface of the beam (the surface towards the compression zone) was not exposed to fire and hence assumed to be insulated during fire exposure. All the specimens were tested unrestrained and without any external load applied on them.

After the beams were positioned in the furnace, the furnace was closed using reinforced aerated concrete slabs (Ytong Wandplatten P4.4/0.5 acc. to DIN 4223 [23]; length 625 mm, width 2800 mm, thickness 100 mm). The fire load was enforced by heating the furnace air temperature according to the standard ISO 834 curve for 1 h and subsequently cooled down to room temperature (T = 20 °C). The burners were shut down at the end of the heating phase and the ventilation ducts were slowly opened. Thereafter, the specimens were allowed to cool down naturally for at least 24 h. The furnace door was opened one day later.

2.5.2. Mechanical loading

This section provides information about the test setup, which was used for the application of mechanical load on beams after the fire exposure. Fig. 4 presents of a typical test setup, where the beams were subjected to four-point bending with the lap splice in the constant moment zone. This setup ensures a well-defined region of uniform bending moment between the load points, isolating shear effects and focusing on flexural behaviour. The components of the test setup comprise: a servo-hydraulic cylinder for applying the load, a calibrated load cell for measuring and monitoring the load, linear variable displacement transducers (LVDTs) for measuring vertical/horizontal displacements and crack widths and a data acquisition system to record the test data.

All the beams were simply supported and loaded to failure in four-point bending under static load. The spacing of the supports was 3m. Fig. 4a presents a schematic diagram of the applied loading during the tests. The two-point load spaced symmetrically from the middle point of the specimen was applied to the beams by using the servo-hydraulic cylinder. The length of the uniform bending moment section, i.e. the loading points at the center of the beam was set to 800 mm irrespective of the presence and length of the lap splice giving a constant shear span of 1100 mm. During the tests the boundary conditions are considered in such a way so that the RC beams are simply supported with a roller support at one side and a hinged support at the other side. A steel spreader beam with two steel roller supports covering the entire width of the beam was used to distribute the load through two-point loads. The load was applied with constant force increment. A teflon sheet was sandwiched between the contact surfaces of the support with the uneven surfaces of the test beams to minimize friction. A calibrated load cell having a maximum load carrying capacity of 100 kN was placed between hydraulic jack and steel girder was connected to data logger to measure the force applied on the beam during the test.

The load was applied to the specimens until the first cracking was observed on the tension side of the beams. The cracks were traced and marked in black while the applied load was held constant. Loading continued in this fashion, with pauses after approximately 10 kN increments thereby allowing a controlled observation of the crack propagation and documentation of the structural response at various stages. The propagation of crack at each step of load increment and the mode of failure were recorded.

Fig. 4b and c presents a close view of the LVDTs placed at different locations of the beam. A total of four LVDTs were mounted vertically at different locations of the bottom surface of the beam. Two of the LVDTs were placed at quarter-span on either side of the loading span, one the loading point and another at the mid span of the beam, with all four LVDTs placed at the bottom surface of the beam. The test setup was also equipped with three LVDTs placed horizontally at the mid span of the beam to measure the curvature.

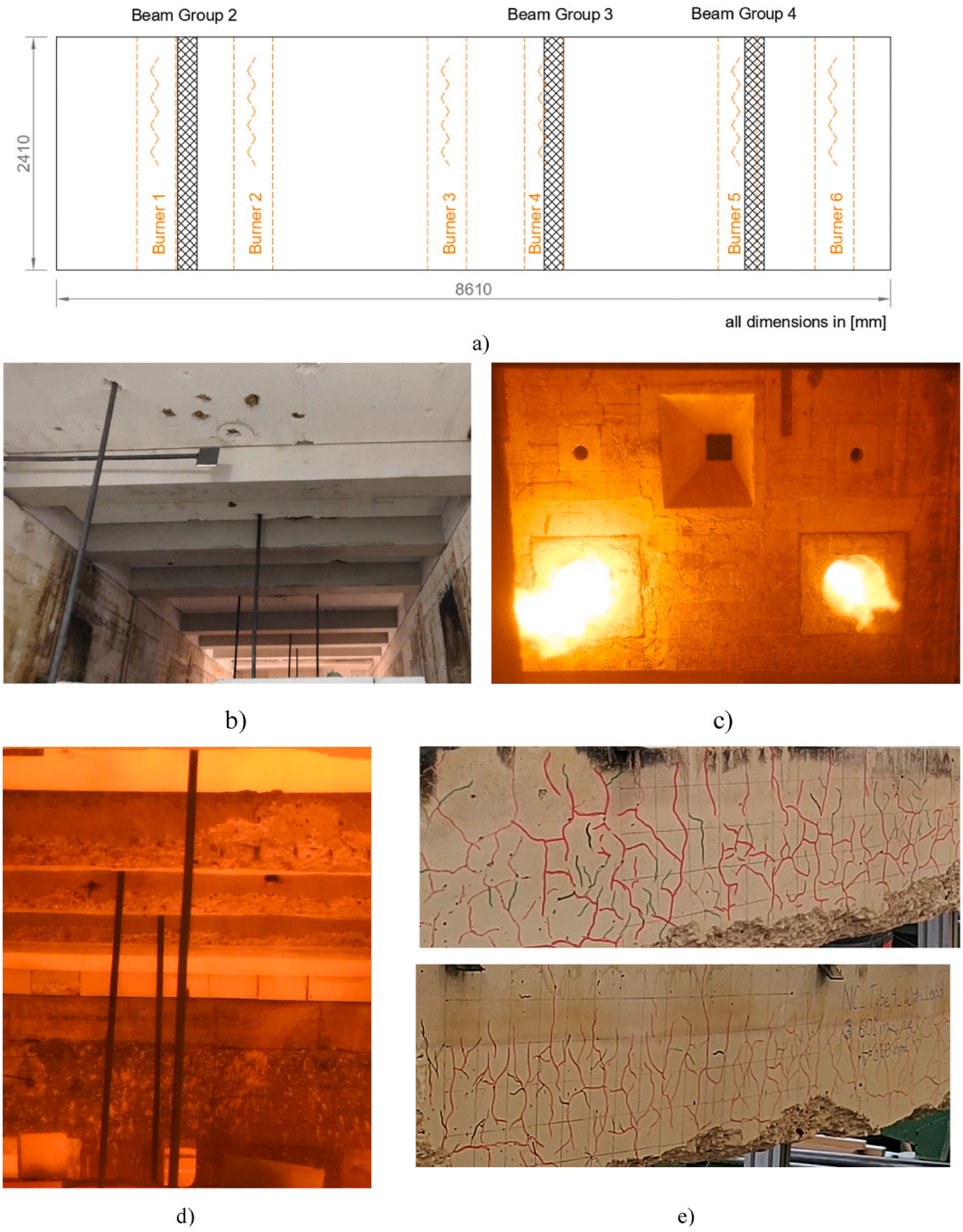

Fig. 3. a) Top view of the furnace, b) inside view of the furnace showing the exposed sides of the beams c) burners, d) view into the furnace during the fire test, e) post-heating thermal damage of the beams.

3. Test result and discussion

3.1. Thermal behaviour

The temperature distribution inside the furnace as well as thermal response of the beams during the fire are presented and discussed in this section. The recorded temperature history obtained from the sheath thermocouples placed at several locations of furnace as well as near the fire exposed surfaces of the beams (thermocouple positions are shown in Fig. 2c) are presented in Fig. 5. The thermocouples are labelled Ext_TC1 to Ext_TC12. Unfortunately, due to a technical error the temperature measurements of two thermocouples

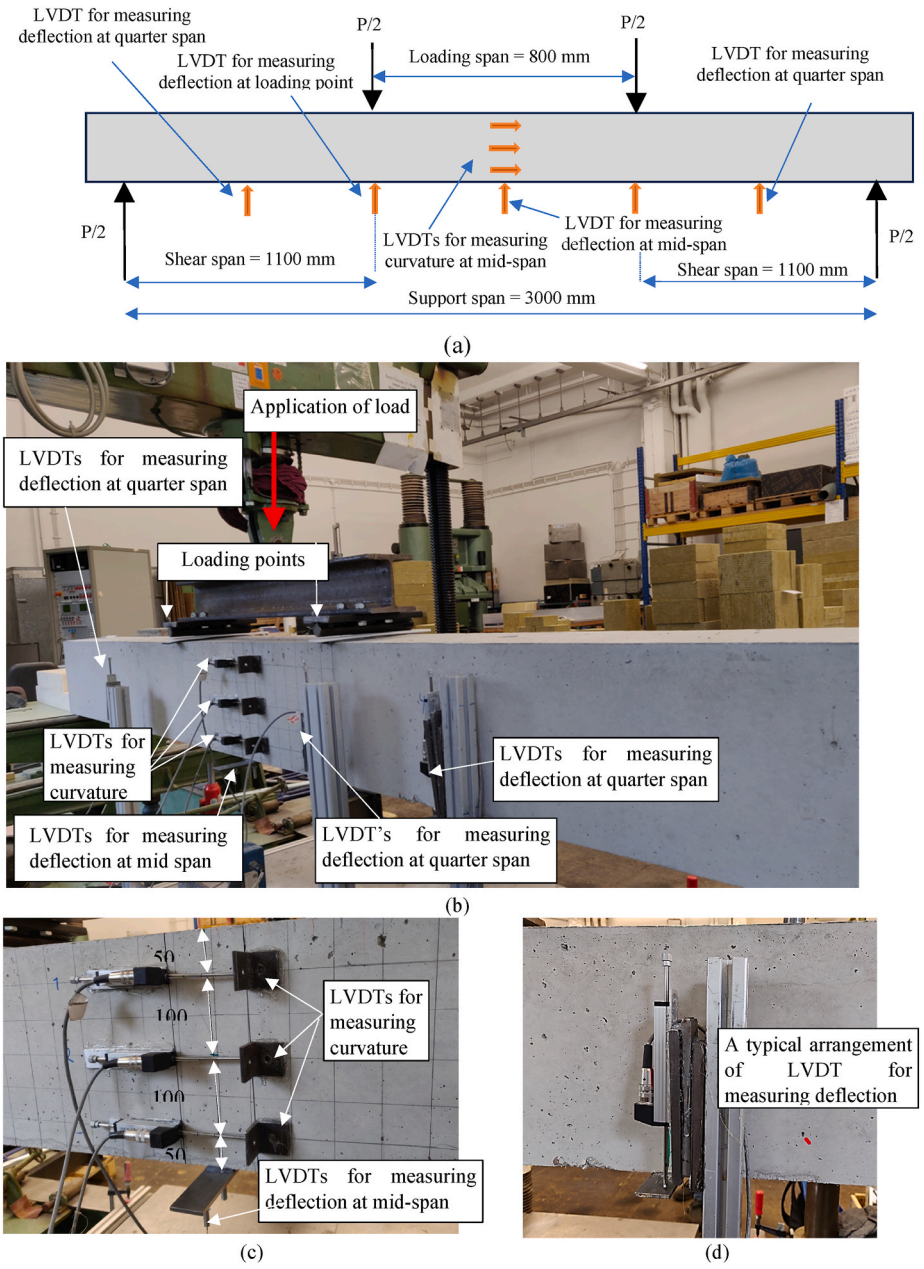

Fig. 4. a) Schematic diagram of the applied loading during the four-point bending test, b) a typical arrangement of the test setup c) placement of LVDTs at the mid span of the beam for measuring the curvature d) a close-up view of the LVDT for measuring the vertical deflection during the test.

(ExtTC11-Ext_TC12) could not be recorded. Note that the graph "average" indicated the mean temperature measurements of the thermocouples within the furnace obtained from the fire tests. As can be seen, while the measured temperature in individual thermocouples slightly deviates from the target temperature, the average temperature profile nearly coincides with the standard fire curve. Upon reaching the target fire duration of 60 min, the burners were shut down and the ventilation ducts were opened, which lead to a rapid temperature drop within the furnace during the initial cooling phase. However, as the cooling phase progressed, the ventilation ducts were subsequently closed, resulting in a more gradual temperature decrease observed in the later stages.

Fig. 6a and b presents a comparison of the furnace temperature vs. time for the group 1 and group 2 beams. The oven temperature and the standard fire temperature are also shown in the same graphs. It should be noted that the "average" curve represents the mean temperature measurements of the thermocouples within the furnace recorded during the fire tests, as also shown in Fig. 5. On the left-hand side, the temperature measurements of the thermocouples placed on the top of the longitudinal rebars (TL) in the tension zone are plotted, whereas on the right-hand side the thermocouples were placed on the stirrup locations (TS). Expectedly, both beam types

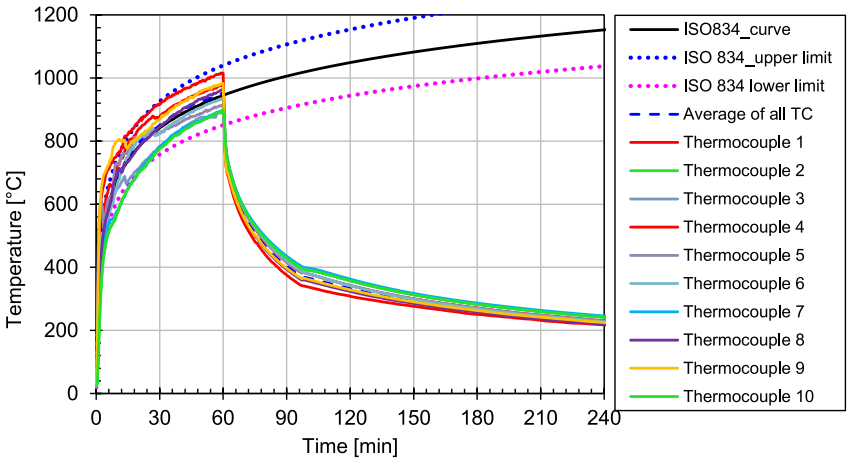

Fig. 5. Temperature inside the furnace during and after the fire test.

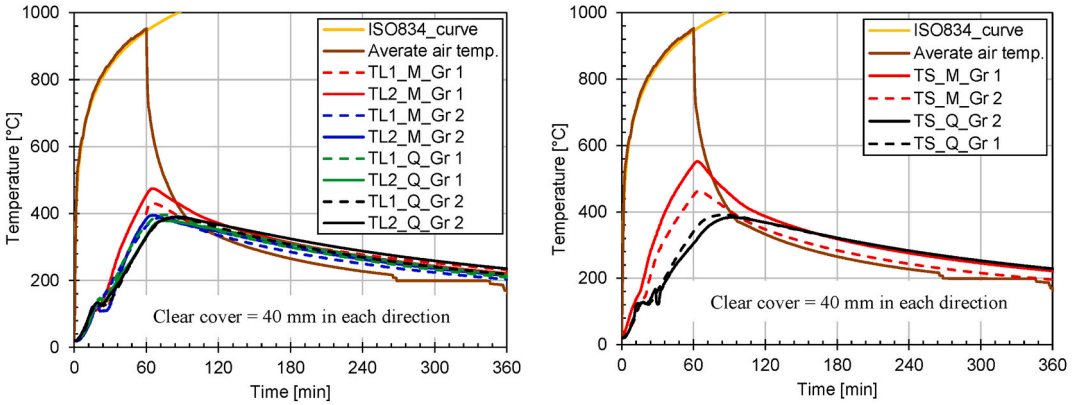

Fig. 6. Temperature measurements inside the concrete layers for 60 min of fire exposure duration a) rebar locations and b) stirrup locations.

exhibit very similar time-temperature curves for the entire heating and cooling phase. The global trend in both the cases reveals that the rate of temperature rise inside the concrete layers is much lower compared to the rise in furnace temperature irrespective of the location of thermocouples, which can be explained by the very low thermal conductivity and high thermal capacity of the concrete playing a crucial role to significantly slow down the heat penetration and to maintain lower temperatures within the inner layers of concrete. This results in a significant temperature gradient within the concrete layers, hence the outer layers try to expand due to heat (free thermal strain), while the inner (cooler) layers tend to restrain this expansion. This differential thermal expansion induces thermal stresses within the concrete, leading to the development of thermal cracks. Certain scatter can be observed in the temperature distribution within concrete, especially in case of thermocouples placed in the mid-span region. For example, the peak temperature of the thermocouple placed at the mid span of the longitudinal rebars of Group 1 beam is around 480 °C and the same is around 400 °C for the Group 2 beam. Similarly, the peak temperature of the thermocouple placed at the stirrups in the mid span region is around 540 °C, whereas the same is around 480 °C for the Group 2 beam. These differences in the temperature distribution inside the concrete layers

Fig. 7. Thermal cracks (marked in red) observed on the beam after the fire exposure.

reflect the differences in the air temperature as well as slight difference in the positioning of the thermocouples.

In the cooling phase, as the fire diminishes and the outer layer of the concrete starts to cool, the temperature gradient reverses since the inner layers of the concrete continue to rise in temperature long after the heating phase has ended. This reversal exacerbates the increment thermal gradient and consequently, the thermal stresses and promotes further damage to the outer concrete layers.

3.2. Fire damage assessment

To understand the severity of the fire impact, a visual inspection was carried out on the fire exposed beam specimens after opening the furnace door. One of the most important observations is the spalling of the concrete in terms of flaking off portions of the concrete surface in the corner regions. This spalling is not explosive spalling but rather corner spalling occurring in the later stages of fire and during cooling.

Another important observation is thermal cracks on the fire exposed surfaces of the beams. Fig. 7 presents the thermal cracks marked on the beam surfaces. In order to identify and analysed the more significant thermal cracks only crack widths of 0.1 mm or greater are marked in this case. As mentioned above, the cool inside portion of concrete restrain the expansion of the heated surface. Moreover, high temperatures cause differential expansion between concrete and reinforcing steel. These effects lead to pronounced surface cracking.

3.3. Results of the four-point bending tests

3.3.1. Group 1 beam

Initially, the authors intended to conduct experimental investigations on both fire-affected and unaffected continuous beams (beams without lap splice). However, since similar investigations were already carried out by Sharma et al. [13], these results are used in the present work in order to reduce testing expenses. Consequently, this section of the paper re-presents the results of the continuous beams, facilitating easier comparison with the results of beams with lap splices, which are the main objective of this paper and are discussed in the following sections.

The geometry of the beams, reinforcement details and material properties of the beams tested by Sharma et al. [13] are the same as in the present study. The primary distinction between the test setup employed by Sharma et al. and the one used in the present study lies in the distance between the loading points. In the setup used by Sharma et al. [13], the distance between the loading points at the center of the beam was maintained as 300 mm, whereas in the current setup, this distance was increased to 800 mm. However, though the change in the distance between the loads primarily influences the shear span of the beams, it does not alter the overall moment capacity, since the beams have identical cross-section. Consequently, the moment-curvature relationship, which is crucial for understanding the flexural behaviour of the beam, can be directly compared across different test setups. Therefore, in this paper, the moment-curvature curves derived by Sharma et al. [13], which consider both fire-affected and unaffected continuous beams are reintroduced in this paper as a reference database for comparing the test results discussed in the subsequent sections. The moment-curvature relationships for the three tested simply-supported beams (no fire, after 60 min and 90 min of fire) are presented in Fig. 8. The beam with continuous reinforcement exhibits no deterioration in terms of moment capacity due to exposure to fire. Even though concrete underwent substantial damage in the concrete cover region and very high maximum temperatures were reached in the longitudinal reinforcement, the residual post-fire capacity is almost unaffected. Regardless of the fire duration, the beams experienced ductile failure due to the yielding of the reinforcement. This limited effect of fire can be explained by the facts that the beams were designed to fail by reinforcement yielding (under-reinforced beam) and the reinforcing steel regains a major portion much of its strength and stiffness upon cooling. The degree of recovery depends largely on the peak temperature reached during the fire. The maximum temperature of steel reinforcement ($T_{max,60min}$ = 550 °C and $T_{max,90min}$ = 650 °C) were not high enough to induce substantial steel damage in residual state. Steel typically exhibits degradation of residual mechanical properties only in case it had

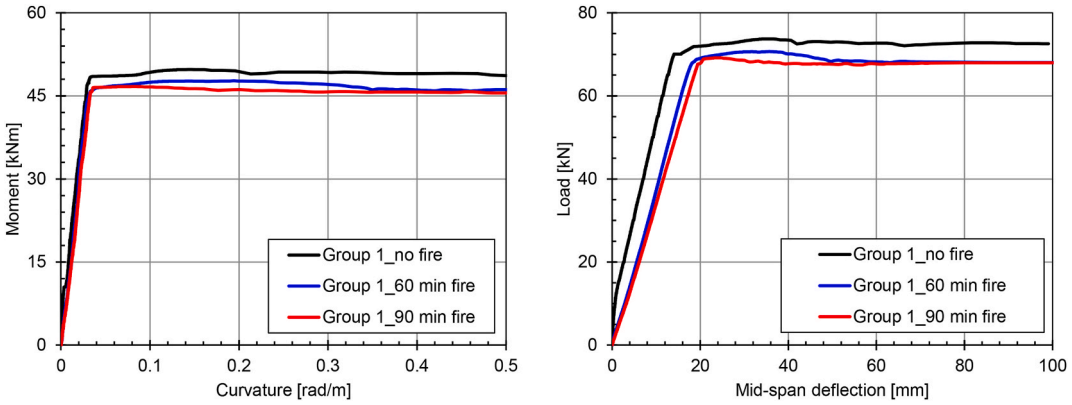

Fig. 8. Moment-curvature (left) and load-deflection (right) response of the Group 1 beams with and without fire exposure (Sharma et al. [13]).

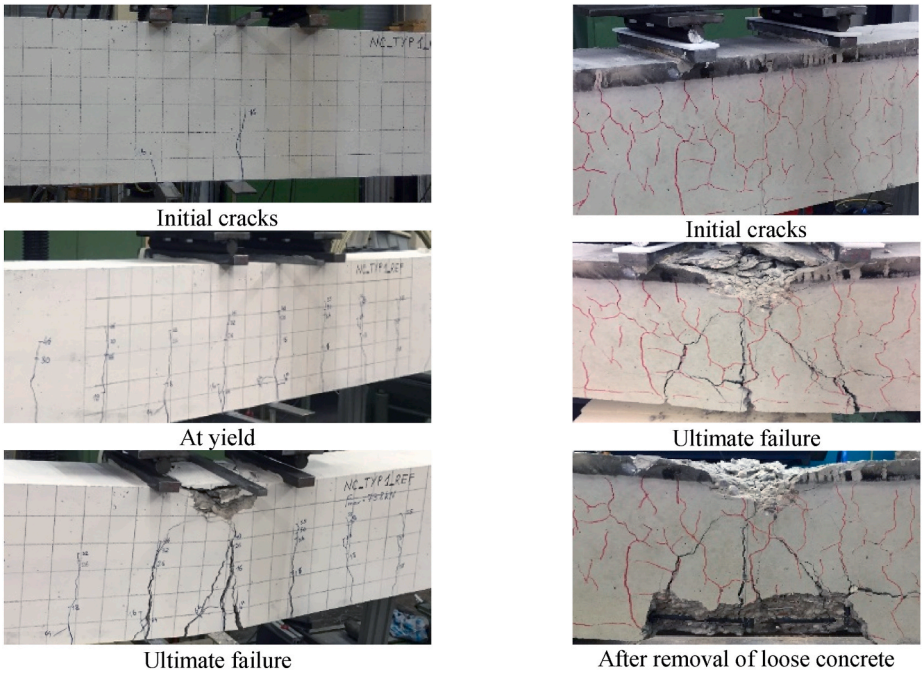

Fig. 9. a) Failure pattern of Group 1 beams: reference (no fire) specimen (left) and fire exposed specimen (right) (Sharma et al. [13]).

experienced temperatures of above 700 °C [13].

3.3.1.1. Failure mode. Fig. 9 illustrates the cracking pattern observed on the Group 1 beam without fire exposure (reference case) as well as fire exposed beams (60 min) [13]. As expected, due to the under-reinforced design and continuous reinforcement, the beams exhibited typical flexural behaviour for both the fire exposed and non-exposed cases, primarily governed by the yielding of the tensile reinforcement, resulting in large crack widths and plastic hinge formation in the mid-span of the beams. Prior to failure, several evenly spaced flexural cracks were observed along the span of the beams.

In case of the reference beam (no fire), initially, vertical flexural cracks appear in the region of maximum moment between the loading points. These cracks start at the tensile face of the beam and propagate upward toward the neutral axis. As the load increases, these cracks widen and extend further. With the further increase of the load, as the tension reinforcement yields, it allows for further deformation. Eventually, concrete in the compression zone reaches its ultimate strain capacity. When this limit is exceeded, the concrete in this region begins to crush locally on the beams top surface.

In the case of fire-exposed beams, vertical flexural cracks generally appear in the mid-span region between the loading points during the bending test, much like those observed in beams that had not been exposed to fire. However, those flexural cracks were primarily the pre-existing thermal cracks caused by fire exposure. Since they initiated during the heating and cooling phases, they continued to expand and propagate until yielding occurred. As with the beam that was not exposed to fire, concrete crushing in the compression zone was also observed.

3.3.1.2. Numerical simulations. Since the experimental investigation of Group 1 beams with continuous reinforcement was not included in the present program, the results reported by Sharma et al. [13] were adopted for reference. Therefore, a complementary numerical simulation of the Group 1 beam was performed to enable a more robust comparison. The outcomes demonstrate that the simulated moment–curvature response of the Group 1 beam is in close agreement with the continuous beam results reported by Sharma et al. [13], thereby validating the consistency between the two approaches. In the following part, a brief description of the numerical simulations including the modelling approach, thermos-mechanical model has been presented.

In the present study, numerical simulations were carried out using the in-house developed three-dimensional finite element software MASA. The constitutive behaviour of concrete was modelled with a temperature-dependent microplane formulation (Ožbolt et al., 2005) [24]. To ensure consistency with the experimental program, the numerical investigation was conducted in two sequential stages: (a) simulation of the fire exposure, including the complete heating and subsequent cooling phase back to ambient conditions and (b) simulation of the post-fire mechanical test (four-point bending) response. In the first stage, a coupled thermal analysis was performed on the beam specimens to determine the transient temperature distribution within the concrete. In the second stage, vertical loading at 800 mm distance was applied on the beam to capture the residual performance following fire exposure.

The microplane model, developed specifically for concrete, characterizes the material response by defining stress–strain relationships on multiple planes of varying orientations. These planes, often referred to as 'weak planes' or 'weak surfaces'—such as the

interfaces between aggregate and cement paste—capture the heterogeneous nature of concrete (Ožbolt et al., 2001) [25]. In this framework, the material behaviour is obtained by evaluating stress and strain components along predefined microplanes and subsequently integrating their contributions to derive the macroscopic stress tensor from a given macroscopic strain tensor. Unlike traditional phenomenological constitutive models for concrete, which typically rely on tensor invariants within plasticity or damage mechanics formulations, the microplane model achieves tensor consistency inherently through the collective response of the microplanes. The version of the model adopted in this study (Ožbolt et al., 2001) [25] is based on the relaxed kinematic constraint concept.

In the thermo-mechanical analysis, the total strain of concrete at elevated temperatures is expressed as the sum of three components:

$$\varepsilon_{total} = \varepsilon_m + \varepsilon_{fts} + \varepsilon_{lits} \quad (1)$$

where, ε_{total} is the total strain, ε_m is the mechanical strain, ε_{fts} is the free thermal strain, and $\varepsilon_{lits\backslash}$ is the load-induced thermal strain (which arises when concrete is subjected to compressive stresses during heating). The mechanical strain itself is further decomposed into elastic, plastic, and damage-related contributions. The temperature dependence of the physical and mechanical properties of both concrete and reinforcing steel is incorporated, with degradation laws closely aligned with the recommendations of Eurocode 2 (Ožbolt et al., 2005) [24]. This constitutive model has been previously validated by Das et al. (2019) [5], demonstrating very good agreement with experimental results for the bond behaviour of single rebars exposed to fire.

For the present numerical simulations, the values of compressive strength, tensile strength, and Young's modulus obtained from the concrete tested under ambient conditions were adopted (see Table 3). Additional thermo-physical properties, including thermal conductivity, specific heat capacity, and free thermal strain, were assigned in accordance with the provisions of Eurocode 2 [7]. Furthermore, the degradation of both the mechanical and physical properties of concrete with increasing temperature was modelled following the temperature-dependent reduction factors recommended in Eurocode 2 [7].

To simulate the fire exposure scenario, the surface nodes of the finite element model were subjected to environmental (air) temperatures defined by the ISO 834 standard fire curve (ISO 834-1, 1999) [17]. The duration of fire exposure was varied from t = 0 to t = 60 min (reference specimens without fire) to the maximum exposure time considered. Consistent with the experimental program, heating was applied to three sides of the beam specimen—the top surface and the two vertical faces—while the remaining surface was left unexposed. In order to ensure direct comparability with the experimental results, the cooling phase recorded during testing was

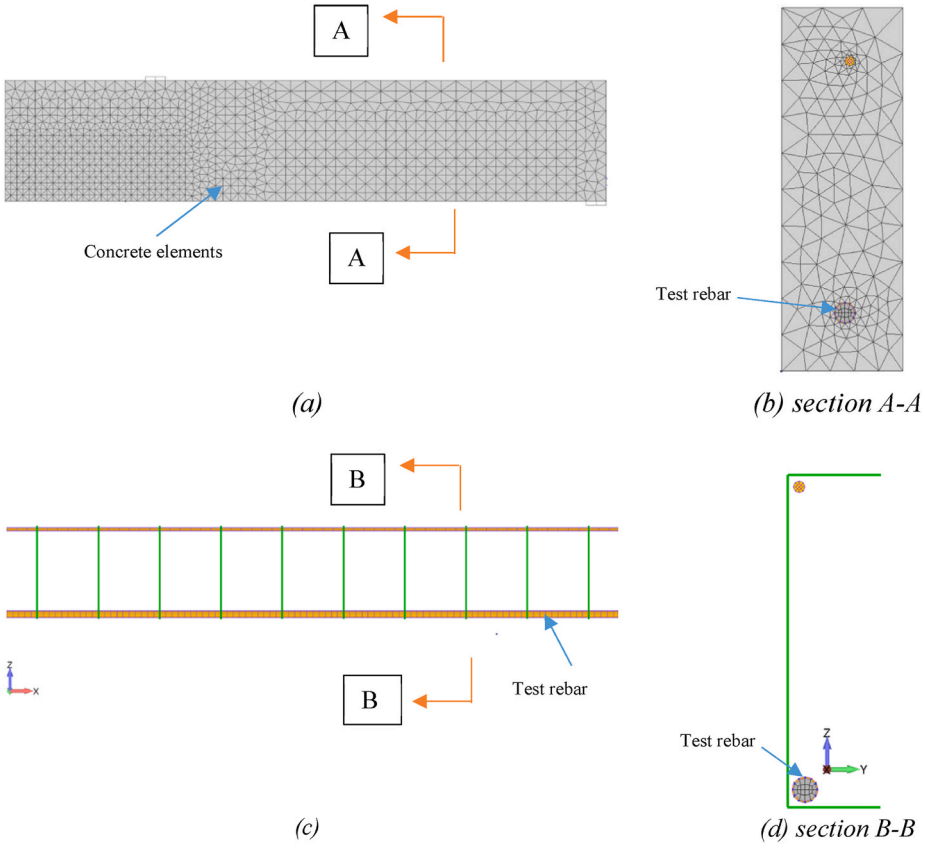

Fig. 10. Finite element model of the beam. a) Complete model of the beam b) Section A-A of the complete model c) Reinforcement-cage and d) Section B-B from the reinforcement cage.

accurately reproduced in the numerical simulations.

The concrete domain was discretized using four-noded tetrahedral solid elements, while the test rebars were represented by eight-noded hexahedral solid elements. Since the primary objective of this study was to investigate the post-fire bond performance of concrete, the material behaviour of the test rebars was idealized as linear elastic. The corner longitudinal rebars and stirrups were modelled with two-noded truss elements to capture their axial response. For reinforcing steel, a tri-linear uniaxial stress–strain relationship was adopted, defined by four key parameters: initial elastic modulus, yield strength, hardening modulus, and ultimate strength. Fig. 10 presents the details of the finite element model of the beam. Note that in order to reduce the total run time half of the beam is modelled.

The interaction between concrete and reinforcing steel in the interfacial region was represented by one-dimensional, two-noded bar elements capable of transmitting only shear and compressive forces. A tri-linear bond–slip relationship was employed to define the uniaxial constitutive behaviour of these elements (see Fig. 11a). The bond stress–slip curve is characterized by the following parameters: , the τ_{max} which is maximum bond stress (pure pull-out strength); τ_R, the residual bond stress; s_1, the slip corresponding to τ_{max}; s_2, the plateau length; and s_3, the slip value at which the residual frictional stress is mobilized in the post-peak branch. Within the bonded region, the maximum bond strength of the interface elements was set to 12 N/mm^2, whereas the de-bonded region was simulated using bar elements with a very low stiffness and a negligible bond strength of 0.1 N/mm^2. As bond deterioration was attributed primarily to concrete damage and relative dilatation between steel and concrete, no explicit temperature-dependent material law was applied to the bar elements. Fig. 11b provides a detailed view of the test rebar, illustrating the use of eight-noded hexahedral solid elements for modelling the rebar itself and two-noded bar elements for representing the bond behaviour along the lap splice length.

3.3.1.2.1. Numerical results. Fig. 12a presents a comparative assessment of the moment–curvature responses obtained from the present numerical simulations and those reported by Sharma et al. [13]. The comparison indicates that, while a slight variation exists in the ultimate moment capacity, the overall shape and progression of the curves show strong consistency. In particular, both studies capture the key stages of structural response, including the yielding of tensile reinforcement, and the subsequent strain-hardening behaviour prior to failure. Both the beams; the one subjected to fire exposure as well as the reference beam tested under ambient conditions, exhibited similar behaviour demonstrating that the numerical framework employed in this study is capable of reliably reproducing the fundamental flexural behaviour of continuous reinforced concrete beams. Similarly, Fig. 12b presents a comparative evaluation of the load–deflection responses obtained from the present numerical simulations and those reported by Sharma et al. [13]. The comparison reveals that, although a slight discrepancy exists in the ultimate load capacity, the overall trends of the two curves are highly consistent, capturing both the elastic and post-yield behaviour with good agreement. The minor variation in ultimate capacity can be reasonably attributed to differences in the distance between the applied loading points in the respective studies, which directly influences the shear span-to-depth ratio and, consequently, the ultimate load-capacity of the beams.

3.3.1.2.2. Failure mode. Fig. 13 presents the cracking patterns obtained from the numerical simulations for both the Group 1 reference beam (unexposed to fire) and the corresponding beam subjected to 60 min of fire exposure. Consistent with the experimental observations reported in [13], the behaviour of these beams was governed by their under-reinforced design and continuous longitudinal reinforcement, which promoted a predominantly flexural response in both fire-exposed and unexposed conditions. In both cases, yielding of the tensile reinforcement controlled the structural response, leading to the development of wide cracks in the mid-span region. Once the rebar yields, the beam undergoes significant deflections, and the cracks in the tension zone continue to widen. As the load approached failure, multiple flexural cracks appeared along the span, distributed relatively uniformly, thereby reflecting the ductile nature of the response. Importantly, the numerical simulations successfully reproduced these features, including the sequence of crack formation, their spacing, and the ultimate flexural failure mechanism. This close correspondence with experimental results confirms the ability of the numerical model to accurately capture the post-fire flexural behaviour of RC beams and validates its reliability for further comparison and consideration of the results of the experimental investigations of Group 1 beams of

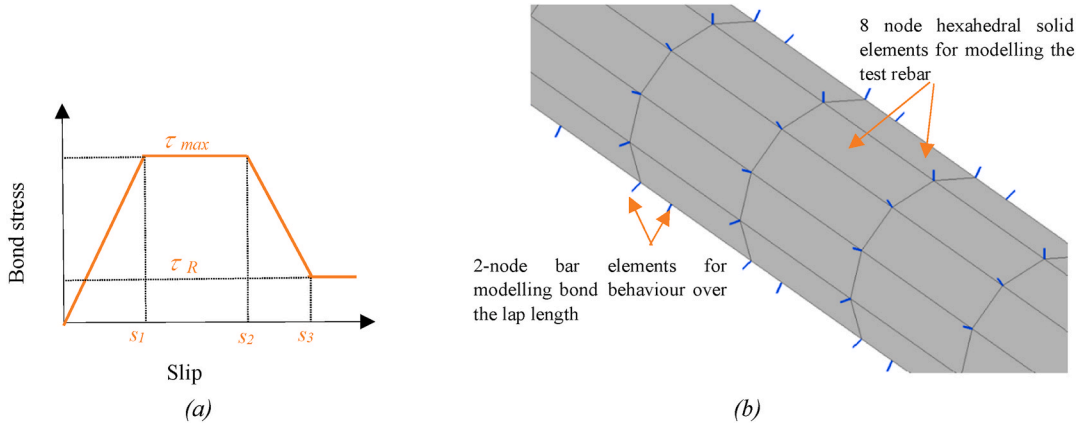

Fig. 11. a) Idealized bond stress–slip relationship used as constitutive law for the 2-node bar elements in the FE analysis. b) A closeup view of the test rebar along with the bond elements.

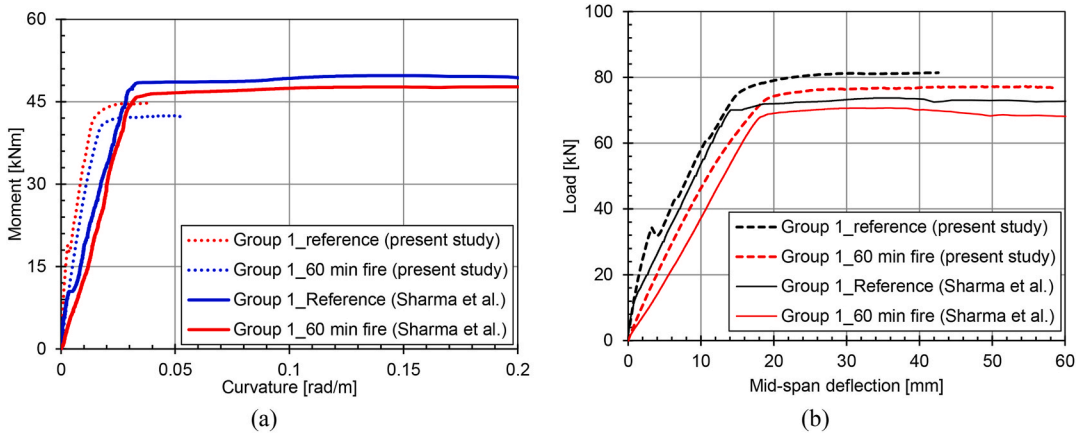

Fig. 12. A comparison of the numerical results of Group 1 beams obtained in this study with the one obtained by Sharma et al. [13]): moment-curvature (left) and load-deflection (right) response.

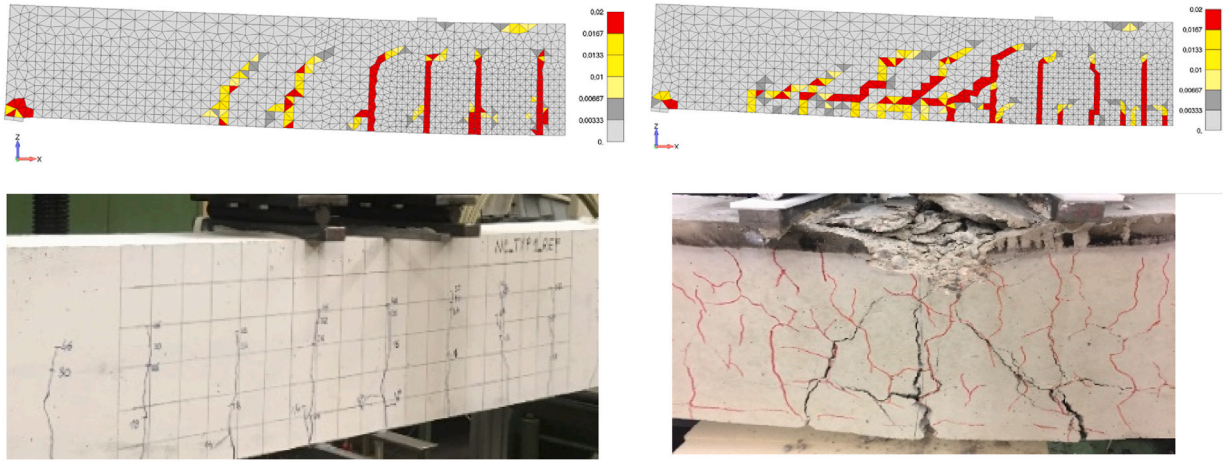

Fig. 13. A comparison of the numeral failure pattern and experimental failure pattern (Sharma et al. [13]) of Group 1 beams: reference (no fire) specimen (left) and fire exposed specimen (right) after ultimate load has reached.

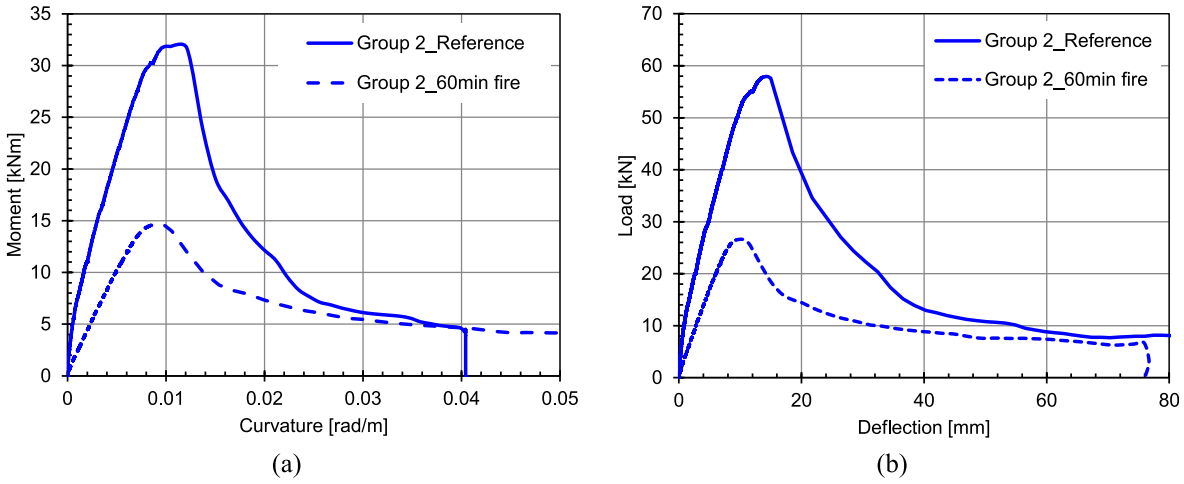

Fig. 14. Moment-curvature (left) and load-deflection (right) response of the (fire-exposed) Group 2 beams.

Sharma et el. [13].

3.3.2. Group 2 beam

3.3.2.1. Moment-curvature. The mid-span moment-curvature behaviour obtained from the four-point bending tests for group 2 beams is presented in Fig. 14a. Note that, κ is the curvature in the constant bending region which is calculated by dividing the sum of the absolute values of the LVDT measurements of the compression zone (δc) and the tension zone (δt) during the bending test by the distance between the compression and tension LVDTs. The details of the LVDTs are presented in Fig. 4. Thus, a linear strain profile is assumed along the depth of the beam. The distance between the two points at which the curvature was calculated was 200 mm (100 mm on each side of the center of the beam), resulting in an average curvature over the beam depth as:

$$K = \frac{|\delta_{c+}\delta_t|}{200} \tag{2}$$

Both reference and fire-exposed beams exhibited similar failure modes. A sudden drop in the moment-curvature curve immediately after reaching the peak load over a relatively small displacement indicates a brittle failure mode, which is attributed to the bond splitting failure between steel and concrete prior to the yielding of the rebar. There is a significant reduction in the ultimate moment capacity of the beam following fire exposure, with a decrease of approximately 50 % as compared to the reference beam. Unlike beam with continuous reinforcement, only a maximum moment of 14.64 kNm (curvature approx. 0.012 rad/m) could be achieved for the fire exposed beam as compared to 31.86 kNm (curvature approx. 0.022 rad/m) reached by the reference beam. This substantial loss in capacity highlights the detrimental effect of fire on the structural performance, thus resulting in a diminished ability to resist applied bending moments. The lower initial stiffness of the fire exposed beam, as compared to its unexposed counterpart can be attributed to the presence of thermally induced cracks due to fire exposure. Therefore, the load applied during the mechanical test primarily widened existing cracks or initiated new cracking from pre-existing weak points within the damaged concrete.

When comparing the moment-curvature relationships between Group 1 (Fig. 8) and Group 2 beams (Fig. 14a), the principal difference lies in the overall response of the beams. Unlike Group 1 beams, the Group 2 beams exhibit a significant degradation of moment capacity in post-fire state due to fire exposure. This is attributed to the fact that in the case of Group 2 beams, the failure is controlled by bond splitting failure, which is governed by the tensile strength of concrete. Since concrete damage is aggravated due to exposure to fire and subsequent cooling, the fire-exposed beam is already subjected to damage in the critical lap splice region prior to mechanical loading and thereby results in reduced bending capacity.

While analysing the moment-curvature behaviour of the reference beam, it can be observed that, at low loads, the moment-curvature curve follows a linear path, as both the concrete and reinforcement remained uncracked and elastic. No significant bond stress developed in the lap splice region yet and the beam behaves as expected under flexural loading. As the load increases, flexural cracks begin to form, particularly in the tension zone between the loading points. The moment-curvature curve became nonlinear as the concrete in the tension zone cracks and the load transfer relies more heavily on the bond between the spliced reinforcement and concrete. Before the reinforcement can yield, the bond between the concrete and the spliced rebar in the lap splice region fails. This bond splitting failure is marked by the appearance of longitudinal cracks along the axis of the tension reinforcement within the lap splice zone. As bond failure progresses, the beam loses its capacity to transfer stress from concrete to reinforcement. This leads to an abrupt post-peak decline in the moment–curvature response and a relatively brittle failure, with little warning prior to the ultimate failure.

The fire-exposed beam shows a similar moment-curvature behaviour. However, due to the impact of fire, the overall capacity is more than halved and the drop in the moment capacity in the descending branch is much more pronounced than in case of the reference beam. Moreover, the increase of curvature is much smaller as compared to the reference beam attributing to the already existing damage during the fire exposure.

To gain a deeper insight into the structural response, load displacement curves are also plotted (see Fig. 14b). In the initial stage, the beam exhibits an elastic response, where displacement increases proportionally with applied load. However, due to temperature-induced damage as well as material degradation, the stiffness of concrete is reduced compared to an unexposed beam. The weakened bond strength at the lap splice region results in premature bond-slip, causing a more gradual increase in load. Unlike unheated beams, no clear yield plateau is observed. After reaching the peak load, the curve immediately enters a steep descending phase, indicating brittle bond splitting failure rather than ductile behaviour. The rapid loss of load-carrying capacity is due to cracking in the concrete around the lap splice, followed by complete bond deterioration and reinforcement slip.

Although Group 1 and Group 2 specimens were subjected to identical fire exposure conditions and nearly comparable test setups, the only distinction being the presence of continuous reinforcement in Group 1 beams and a lap splice in Group 2 beams, the latter exhibited significantly greater degradation. This heightened vulnerability can be attributed to the lap splice region, where thermal damage during the heating and cooling cycles becomes particularly severe and localized. The bond between overlapping rebars and the surrounding concrete is inherently sensitive to temperature-induced deterioration, as the splice relies solely on bond stresses for force transfer. Elevated temperatures reduce the tensile strength of concrete, impair adhesion, and initiate microcracking at the steel–concrete interface. Additionally, differential thermal expansion between steel and concrete generates interfacial stresses, while the relatively thin concrete cover around spliced regions increase the likelihood of spalling and concentrated heating. During cooling, mismatch in contraction further amplifies tensile stresses, exacerbating crack propagation and permanently weakening the anchorage mechanism. As a result, the lap splice zone emerges as a critical weak link where thermal effects accumulate, leading to localized bond failure and a disproportionately large reduction in the post-fire load-carrying capacity of Group 2 beams.

3.3.2.2. Failure mode. Fig. 15 presents the crack patterns obtained from the four-point bending test of Group 2 beams (reference beam and fire exposed beam) at different stages of the test, I) observation of the first crack, II) before the peak load, III) at the peak load and IV) at the ultimate load. The development of cracks at each stage of loading (every 10 kN) was monitored, marked, and measured on the beams until the load level at which new cracks did not occur. When comparing the failure mode of the reference beam without a splice (Group 1), the failure mode shifts from a ductile flexural failure in Group 1, driven by the yielding of the rebar in the tension zone, to a brittle failure in Group 2 beams, caused by bond splitting failure in the lap splice region. This change in failure mechanism was associated with the rapid loss of bond capacity, which prevented the effective transfer of stress between the overlapping rebars, thereby limiting the overall ductility and energy absorption capacity of the beams. It should also be emphasized that the bond failure observed in the Group 2 reference case was predominantly attributable to the insufficient lap splice length, which did not satisfy the minimum anchorage requirements prescribed by design standards, thus highlighting the critical role of adequate splice detailing in ensuring ductile behaviour and underscores the vulnerability of under-designed splice regions to brittle, bond-dominated failure modes.

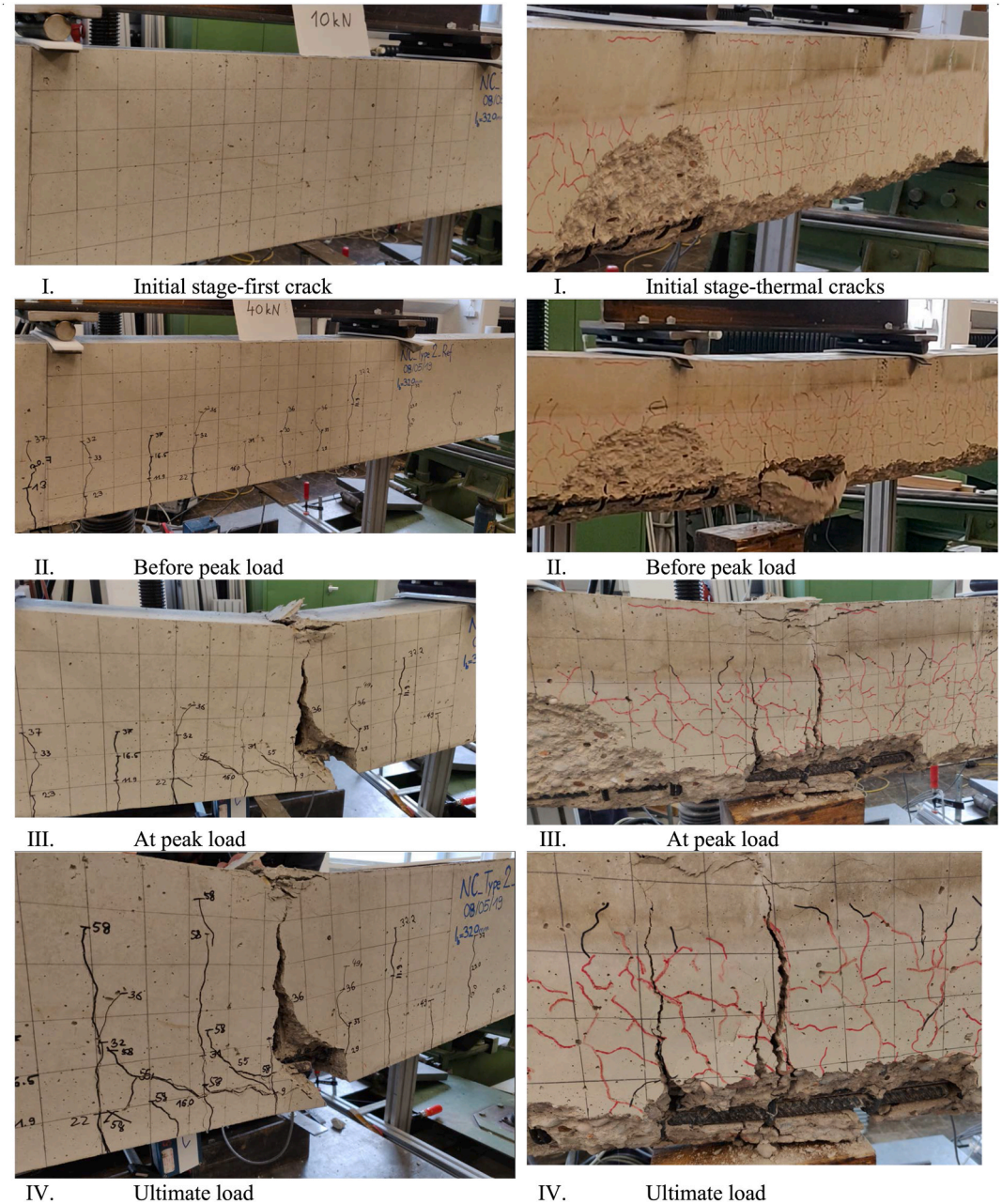

Fig. 15. Failure pattern of Group 2 beams a) reference specimen (left) and b) fire exposed specimen (right).

Group 2 reference beam experienced initially typical bending cracks, similar to group 1 beam. Thereafter, vertical cracks formed at the end of the lap splice region in the tension zone of the beam which then propagated towards the top surface of the beam as depicted in Fig. 15(left). The bond failure was evident from the longitudinal crack running along the axis of the tension reinforcement within the lap splice region. Similar longitudinal cracks were also visible in the bottom side of the beam (not show in photos). In the final stage, concrete crushing in the compression zone was also evident on the top surface of the beam.

Similarly, when comparing the failure mode of the fire-exposed beam without a splice (Group 1), the failure mode once again transitions from a ductile flexural failure in Group 1 to a brittle failure in Group 2 beams, driven by bond failure in the lap splice region, same as the case of reference beam discussed above. However, fire has a significantly stronger impact on the lap spliced beam (group 2) leading to a more premature crack propagation and brittle crack pattern, with wider and more irregular cracks, especially concentrated in the splice area where the bond strength has been deeply compromised. Moreover, removal of cover concrete (bottom cover as well as side cover) around the splice even before reaching the peak load was also observed.

These results are in good agreement with the results presented by the authors on the beam-end specimens regarding local bond strength behaviour (short bond length) [1–5]. This underscores the critical need to account for bond splitting failure while designing the length of a lap splice in the RC flexural member. A shorter splice length can significantly increase the risk of brittle failure, which can result in a sudden and unanticipated collapse, providing little to no warning before failure occurs. Proper design of the lap splice length is essential to ensure ductile behaviour and enhance structural safety.

3.3.3. Group 3 beam

3.3.3.1. Moment-curvature. Fig. 16a presents the moment-curvature plot of the Group 3 beams both for ambient condition and fire exposed condition. Despite the larger splice lengths contributing to higher ultimate moment capacities in both the fire-exposed and unexposed beams compared to the Group 2 beams, the key observation remains the substantial reduction in capacity after fire exposure. Specifically, the ultimate moment capacity of the fire-exposed beam again saw a significant drop of about 50 % compared to the unexposed beam, highlighting again the detrimental impact of fire on the structural performance.

For the unexposed beam, the most important observation is the change of failure mode from bond splitting (brittle failure) in Group 2 to the yielding of rebar in the tension zone in Group 3 (ductile failure). During the analysis of the moment-curvature behaviour observed in the test at the onset of loading, both the concrete and the reinforcement behave elastically, resulting in a linear moment-curvature relationship. The beam deflects within the elastic range, and the curvature increases proportionally with the applied moment. With the further increase of the load, the moment-curvature curve deviates from linearity, as the concrete in the tension zone cracks, and the tensile reinforcement begins to carry more load. As the load continues to increase, the tensile reinforcement in the tension zone reaches its yield point. At this stage, the moment-curvature response becomes highly nonlinear, with a significant increase in curvature for relatively small increases in moment. The yielding of the rebar is a ductile process, allowing the beam to undergo large deformations without a significant reduction in load-carrying capacity. The beam maintains its ability to resist further increases in moments through the plastic deformation of the reinforcement. After the rebar yields, the moment capacity reaches its maximum limit, and the beam exhibits significant deflection and curvature. The lap splice length, being sufficiently long, ensures that bond failure does not occur, and the failure mode is dominated by the ductile yielding of the reinforcement. This behaviour allows for large deformation and provides warning prior to failure. Eventually, as the curvature continues to increase, the concrete in the compression zone reaches its ultimate strain capacity, leading to crushing of the concrete. The moment-curvature curve flattens out, and the beam ultimately fails in a ductile manner, with the yielding of the rebar governing the failure mode. Sufficiently long lap splice ensures that bond integrity is maintained throughout the loading process, preventing premature bond failure, and allowing the reinforcement to fully develop its

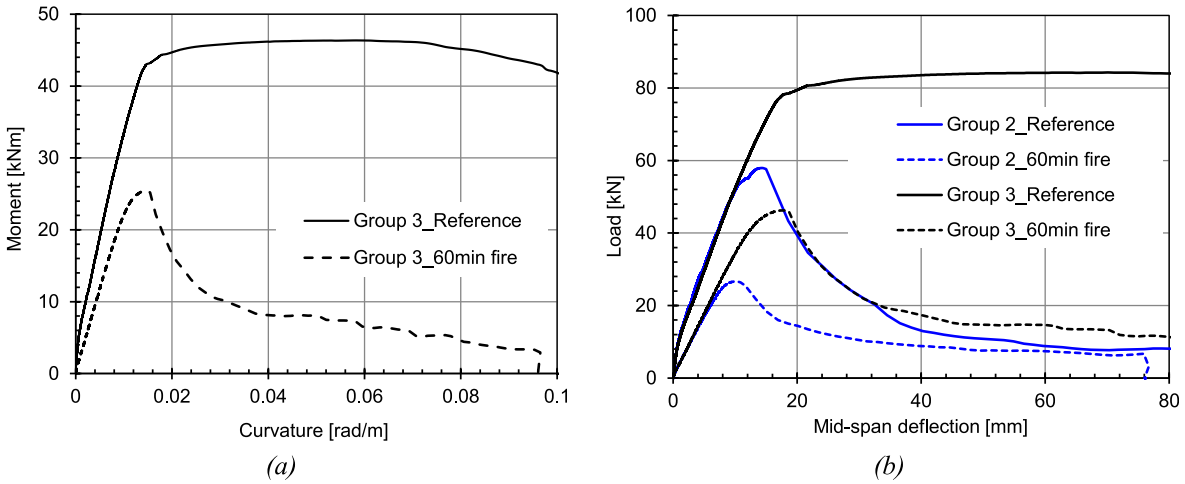

Fig. 16. a) Moment-curvature and b) load-deflection response (fire-exposed) of the Group 3 beams.

strength.

In contrast to the unexposed beam, where rebar yielded before failure thus allowing stress redistribution and progressive deformation, the fire-exposed beam showed a significant shift in behaviour. At the initial stage, the load-deflection curve begins with a linear relationship as the beam responds elastically. No significant deflection is observed, and the bond between the concrete and reinforcement remains intact initially. As the load increases, flexural cracks form in the tension zone, particularly near the lap splice region. The cracks initiate earlier than in the unexposed beam due to the thermally induced concrete damage. Curvature increases more rapidly as the cracks propagate. Instead of yielding of the rebar, the bond between the concrete and reinforcement in the lap splice zone fails prematurely due to the compromised bond strength from fire exposure. This results in a sudden loss of load-carrying capacity and a brittle failure, thus severely reducing the moment capacity of the beam. This emphasizes the detrimental impact of fire on both strength and failure characteristics of reinforced concrete. Additionally, the similarity to the Group 2 beam behaviour suggests that even a splice length increase to $15d_s$ is insufficient to achieve ductile failure after a fire exposure duration of 1 h. However, as the splice length is greater in beams of Group 3 compared to the Group 2 beams, the former display higher moment capacity and initial stiffness.

The load-displacement curve of a Group 3 beam (see Fig. 16b) exhibits a behaviour similar to that of Group 2 beams, with some notable differences. It is visible from the curves that the reference group 3 beam exhibits ductile failure whereas reference group 2 beam exhibits bond splitting. After exposure to fire, both beam types exhibit bond failure.

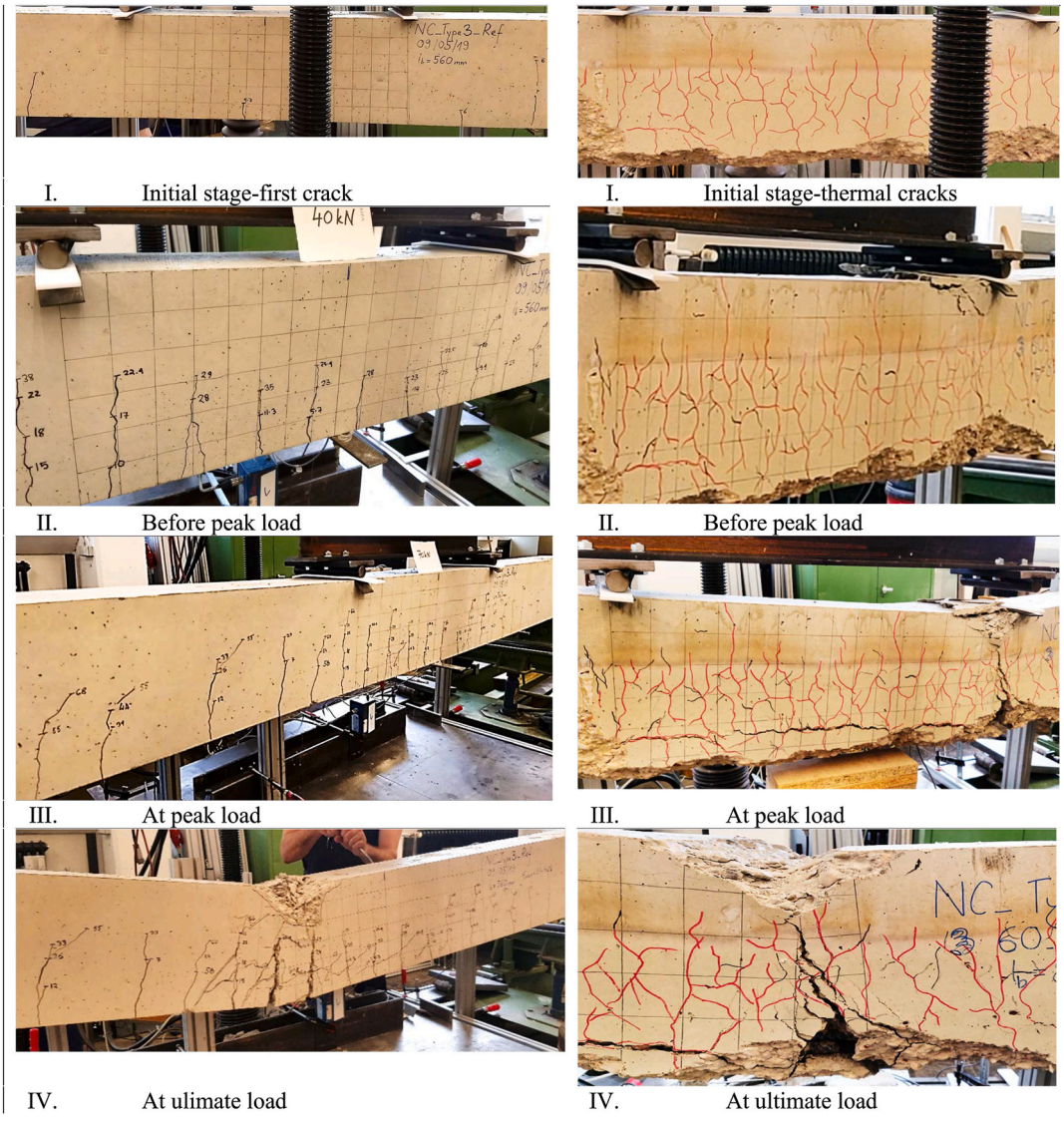

Fig. 17. Failure pattern of Group 3 beams a) reference specimen (left) and b) fire exposed specimen (right).

3.3.3.2. Failure mode. Fig. 17 presents the crack patterns obtained from the four-point bending test of Group 3 beams (reference beam and fire exposed beam) at different stages of the tests. When comparing the failure mode of the reference beam of the Group 2, the failure mode shifts from a brittle failure in Group 2, driven by the bond failure in the lap splice region, to a ductile failure in Group 3 beams, caused by yielding of the rebar in the tension zone.

At the onset of loading, no cracks are present, and the bond between concrete and reinforcement in the lap splice region remains intact. As the load increases, flexural cracks begin to form in the mid-span region, particularly in the tension zone between the loading points. These cracks initiate at the tension face and propagate upwards toward the neutral axis. With the further increase of load, the reinforcement in the tension zone reaches its yield strength. The yielding of the rebar allows for further deformation of the beam, which is reflected in the widening of the flexural cracks. Once the rebar yields, the beam undergoes significant deflections, and the cracks in the tension zone continue to widen. The long lap splice length ensures that the bond between the reinforcement and concrete remains intact, allowing the rebar to fully develop its tensile capacity without bond failure. As the beam continues to deform, the concrete in the compression zone (at the top of the beam) eventually reaches its ultimate strain capacity. This results in crushing of the concrete, marking the final stage of failure. Crushing is localized in the region near the loading points where the compressive stress is highest.

3.3.4. Group 4 beam

3.3.4.1. Moment-curvature. Fig. 18a presents the moment-curvature response of the Group 4 beams subjected to a four-point bending test, highlighting the influence of an increased lap length of $50d_s$ in fire-exposed conditions. Though, similar to Group 3, the failure mode transitioned from a ductile mechanism, characterized by rebar yielding, to a brittle failure due to bond splitting in the lap splice region, the performance exhibit significant improvement compared to the fire-exposed beams of Group 3. The fire-exposed Group 4 beam demonstrated a higher resistance, attaining a peak moment of 42.1 kNm, which is approximately 78 % of the peak moment observed in the reference beam (54.1 kNm). Additionally, the initial stiffness response was notably higher than that of the Group 3 fire-exposed beams.

For the reference beam (no fire exposure), the failure mode was distinctly ductile, governed by the yielding of the rebar. Comparing the reference beams of Groups 2 to 4 it is evident that increasing the lap length generally improves the bond strength between concrete and reinforcing steel under ambient conditions by providing a greater surface area for stress transfer. However, in fire-exposed beams, this beneficial effect can be significantly diminished due to the degradation of bond strength caused by fire exposure. As a result, the extended lap splice may no longer provide the expected improvement in bond performance, leading to premature bond failure.

As previously discussed in the moment-curvature response, the load-displacement curve (see Fig. 18b) of a Group 4 beam exposed to fire exhibits notable enhancements in load-bearing capacity and stiffness, outperforming other fire-exposed beams. The ascending portion of the curve exhibits a steeper slope, reflecting the slightly higher initial stiffness due to the extended lap length, which enhances load transfer between spliced bars. The load increases steadily, reaching a peak almost equal to the reference beam before failure mechanisms initiate. Following the peak load, the curve shows a sudden drop, indicating bond splitting failure and the onset of rebar slip. However, unlike Group 3 beams, the residual load capacity in the post-peak region is significantly higher, which indicates that the beam can still sustain a considerable portion of the load before complete failure.

3.3.4.2. Failure mode. Fig. 19 presents the step-by-step photos of failure obtained from the four-point bending test. Similar to the beams of other group, the thermal cracks visible on the surfaces obtained from the fire tests are marked prior to the machinal loading test. As all the beams were exposed to fire for the same duration, the obtained thermal cracks are very similar as observed in other

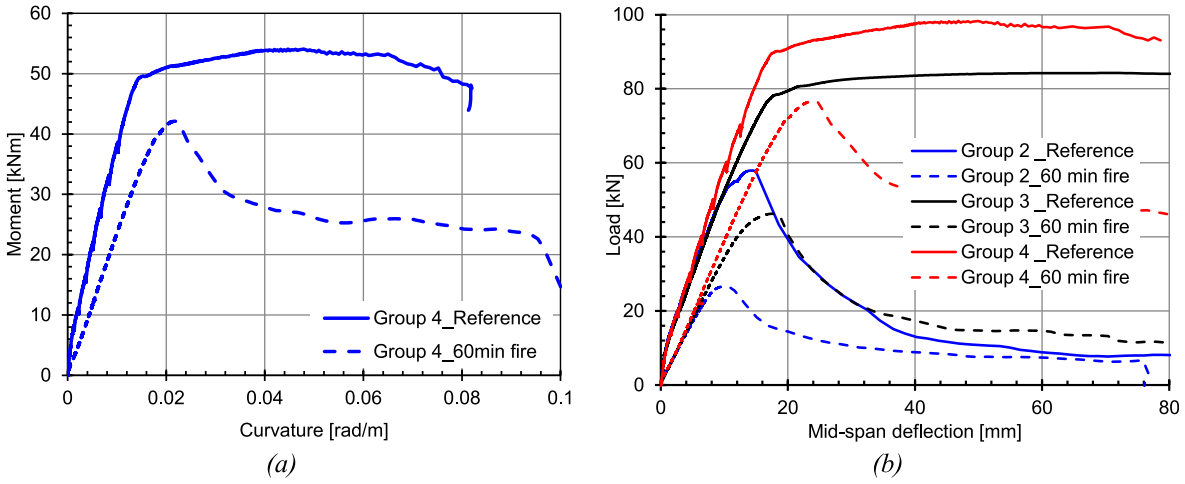

Fig. 18. a) Moment-curvature and b) load-deflection response (fire-exposed) of the Group 4 beams.

Fig. 19. Failure pattern of Group 4 beams a) reference specimen and b) fire exposed specimen.

beams with spliced reinforcement.

Fig. 20a presents relative capacity as a function of lap splice length, with relative stiffness also plotted for a comprehensive understanding of structural behaviour. To enhance clarity, relative stiffness is displayed on the secondary y-axis, allowing for a distinct representation of both parameters and their interdependence. Fig. 20b presents relative capacity as a function of fire exposure

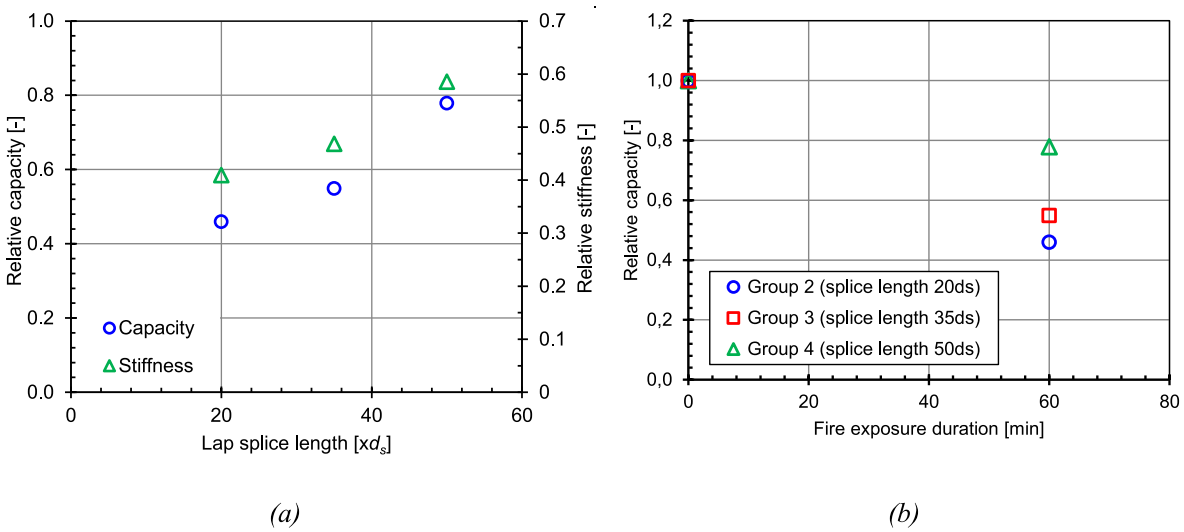

Fig. 20. a) Relative post-fire capacity and stiffness as a function of lap-splice length of all investigated beam groups and b) Relative post-fire capacity as a function of fire exposure duration.

durations. The data illustrates a clear trend where both relative capacity and relative stiffness increase with an extension of the lap splice length, emphasizing the crucial role of sufficient splice length in maintaining the structural integrity of reinforced concrete (RC) members. As can be observed, group 1 beams retained 46 % of their post-fire capacity, Group 2 beams retained 55 %, and Group 3 beams retained 78 %.

At shorter lap splice lengths, both capacity and stiffness remain relatively low, indicating inadequate bond strength and inefficient stress transfer between spliced reinforcement bars. This limitation can lead to premature failure after the fire exposure when bond degradation accelerates due to elevated temperatures. Shorter splice length results in stress concentrations at the splice region, which can lead to a bond failure and a sudden loss of load-carrying capacity, increasing the risk of brittle failure. As the lap splice length increases, a notable improvement in both capacity and stiffness can be observed. The enhanced bond area facilitates a more effective stress transfer between reinforcement bars, thereby improving the load-bearing capability and overall rigidity of the structure. The increasing trend in relative stiffness suggests that longer lap splices contribute to a more stable structural response under load, reducing deflections and minimizing the risk of sudden failure. Additionally, a higher relative capacity with extended splice lengths implies that the reinforced concrete members can sustain higher loads before reaching failure, thus ensuring better structural performance. Nevertheless, all tested beams underwent a brittle bond splitting failure after exposure to fire.

In general, the results for beams with spliced reinforcement exposed to standard fire (ISO 834) correlate well with the results presented by the authors on the beam-end specimens also exposed to standard fire for different fire exposure durations considering local bond strength [1–5], where it was shown that with realistic boundary conditions, bond splitting almost always dominates over other failure modes. This observation is critical for the design of reinforced concrete (RC) flexural members, particularly in fire-prone environments, as it underscores the importance of properly designing the lap splice length to ensure structural integrity.

One of the primary concerns in such conditions is the risk of brittle failure due to inadequate lap splice length. A shorter splice length reduces the bond area available for stress transfer between spliced bars, increasing the likelihood of sudden failure. Brittle failure is especially dangerous in structural applications as it occurs without warning and offers little time for intervention, potentially leading to catastrophic collapse. In contrast, ductile failure provides visible signs of distress, allowing for stress redistribution and progressive failure, which enhances structural resilience. To mitigate these risks, it is crucial to properly design the lap splice in fire-exposed RC flexural members. Adequate splice length ensures sufficient stress transfer and bond strength retention under elevated temperatures, while enhanced confinement measures, such as transverse reinforcement (stirrups or ties), can further prevent bond splitting failure. Incorporating fire-resistant materials and adopting performance-based fire design strategies can significantly improve the overall safety and durability of RC structures in fire conditions.

The findings reinforce the importance of accounting for bond splitting failure in structural fire design, emphasizing the need for robust design strategies to prevent premature failure. By ensuring adequate lap splice length and adopting appropriate fire-resistance measures, engineers can enhance the structural safety, durability, and resilience of RC flexural members, reducing the risk of sudden and unexpected failures in fire-prone environments.

4. Comparison of the results with the model code 2020 design/assessment model for splice/anchorage after fire

Based on the results of experimental and numerical investigations carried out on beams with critical lap splices (Sharma et al. [13]). Tonidis et al. [14]), a model is developed to estimate the residual post-fire bond resistance of reinforcement in concrete, and to design the laps for fire resistance (fire rating). The design concept has been included in the fib Model Code 2020 [15]. The concept of the

model is briefly explained below.

It is acknowledged that all the tests were carried out on unloaded bars. However, tests by Muciaccia and Consiglio [26] and their direct comparison with the tests by Sharma et al. [27] showed that when the applied mechanical load during heating on the bars is limited to 60 % or lower of its bond strength under ambient conditions, the effect of mechanical load during heating on the residual bond capacity is negligible. Since the ultimate design loads are typically restricted to approx. 50 % of the mean resistance, it is assumed that the effect of mechanical load during fire can be ignored.

The reduction shown in Fig. 21a is valid for local bond strength (short bond length, Das et al. [3]). In reality, the splice lengths in reinforced concrete members are rather high, with a typical range of 40–50 bar diameters. At such long bond lengths, the distribution of bond stresses is highly nonlinear even under ambient conditions, with a strong possibility of re-distribution of bond stresses along the length of bars. In case of fire, these effects can be further aggravated. Experimental investigations and numerical simulations on beams with lap splices (Tonidis et al. [14])showed that the higher the lap splice length, the more gradual is the reduction of residual post-fire bond capacity of the lap splice (Fig. 21b). The findings from the present study have been compared with the numerical results reported by Tonidis et al. [14], revealing a notable trend. Specifically, the experimental results indicate a slightly higher post-fire capacity of the beam compared to the numerically obtained values. This discrepancy could be attributed to inherent differences between experimental conditions and numerical modelling assumptions, including material properties, thermal effects, and bond degradation mechanisms. Nonetheless, the overall agreement between the two sets of results validates the numerical approach.

Based on the evaluation of lap splice tests, the reduction factors, β_{fi}, for post-fire bond resistance of lap splices were proposed (Table 4). Assuming that the scatter in the test results in post-fire conditions is similar to the scatter in the test results under ambient conditions, the factor β_{fi} can be simply applied on the characteristic resistance as well. Thus, in the case of assessment of a lap splice in a fire affected existing structure, the residual characteristic resistance of the lap splice can be obtained by multiplying the ambient characteristic resistance of the lap splice with the factor β_{fi} as

$$R_{k,fi} = \beta_{fi}\, R_{k,amb} \tag{3}$$

Fig. 22 presents the relative residual capacity as a function of fire duration for different lap lengths, comparing the results reported by Tonidis et al. [14] with those obtained in the present study.

However, in Europe, the design bond resistance is obtained by dividing the characteristic resistance with the partial safety factor for concrete, γ_{Mc}, which takes the value of 1.5 under ambient conditions but can be taken as 1.0 for fire (accident) scenario. Therefore, the design fire resistance, $R_{d,fi}$ of a lap splice or an anchorage can be taken equal to its characteristic resistance $R_{k,fi}$. The design of a lap splice or an anchorage for a particular fire rating can then be performed by ensuring that the post-fire resistance of the lap splice or an anchorage is greater than the design action in case of fire. It is likely that for higher fire ratings (beyond 60 min), the splice/anchorage lengths might need to be amplified to account for the effects of fire.

5. Conclusion

The principal focus of the study presented herein was to understand the bond behaviour of reinforced concrete beams with a lap splice in the tension zone after fire exposure. Beams with spliced reinforcement with lap lengths ranging from 20 to 50 times the bar diameter were investigated experimentally. Following procedures similar to previous studies on the beam-end specimens, the beams were exposed to ISO 834 [17] fire scenario for the desired durations and subsequently allowed to cooled down naturally to the room temperature. Thereafter, the beams were subjected to four-point bending tests. The results were compared to beams with continuous reinforcement (no lap splice) to evaluate the impact of splicing. Additionally, reference beams (not exposed to fire) for each lap length were tested to isolate the effects of fire on bond strength and failure modes. Based on the obtained results, following conclusions can be derived:

1. Fire exposed beams with continuous reinforcement maintained their flexural capacity and displayed a ductile failure mode characterized by steel yielding. In contrast, fire exposed beams with lap splices experienced a significant loss in capacity and exhibited a brittle bond splitting failure mode. This shift in failure mode emphasizes the adverse effects of fire exposure on beams with lap splices, highlighting the need for careful consideration of lap splice design with respect to performance in fire.
2. All fire-exposed beams showed a significant reduction in the ultimate moment capacity and a limitation to its deformation ability. However, with the increase in the lap splice length from $20d_s$ to $50d_s$, an increase to the reduction in the ultimate moment capacity from 50 % to 78 % could be observed.
3. Relative degradation of stiffness (corresponding to one third of the peak moment) follows a similar pattern as the degradation of flexural capacity.
4. The findings for beams with spliced reinforcement align well with previous studies on local bond strength, demonstrating that bond splitting failure is the predominant mode under realistic boundary conditions. However, the post-fire capacity of beams with relatively long splices is higher than assumed by the model. These results highlight the crucial importance of considering bond splitting failure when determining lap splice lengths in reinforced concrete (RC) flexural members as insufficient splice length can lead to a brittle failure mode, significantly increasing the risk of sudden and unexpected collapse, with minimal warning.
5. It should be noted that the beam tests in this work were performed with only one specimen per case considering the high cost and time associated with the manufacturing, storing and testing of full-sized structural elements. However, the previous studies by authors conducted using the beam-end specimens showed that the scatter of the test results in post-fire conditions was not worse

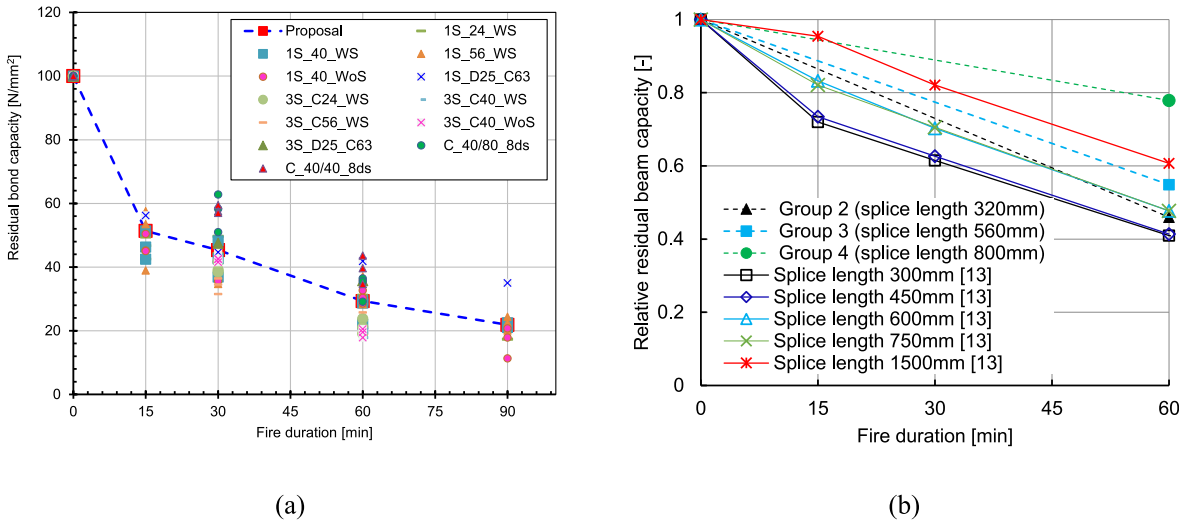

Fig. 21. a) Relative residual bond capacity as a function of fire exposure durations for all the investigated specimen considering beam-end specimen (Das et al.) [3] (left) b) Relative bond strength of lap splices with different splice lengths (taken from Tonidis et al. [14](right).

Table 4
Reduction factor for calculating post-fire bond resistance considering different fire exposure durations.

Exposure duration as per ISO 834-1 [min]	Residual capacity *(βfi)* [−]
0	1.00
15	0.80
30	0.68
60	0.45
90	0.35

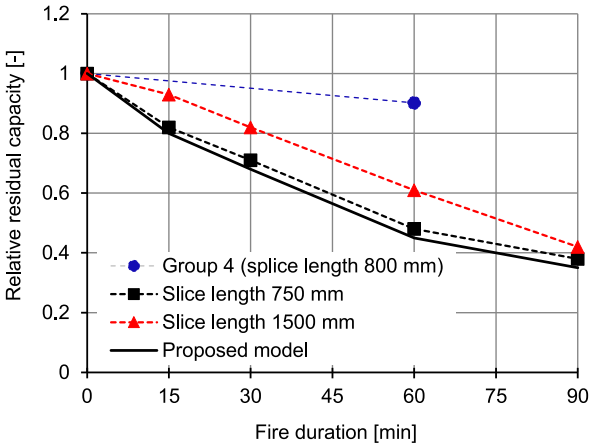

Fig. 22. Relative residual capacity as a function of fire duration for different values of the lap length (partly taken from Tonidis et al. [14].

than the typical scatter associated with the concrete failure modes under ambient conditions. Therefore, the same scatter as generally considered for ambient conditions and concrete related failure modes was assumed to develop the design model. A more robust reliability analysis was out of scope of this work, and is highly recommended.

CRediT authorship contribution statement

Arunita Das: Writing – original draft, Investigation, Conceptualization. **Josipa Bošnjak:** Writing – review & editing, Resources,

Investigation, Funding acquisition, Conceptualization. **Akanshu Sharma:** Writing – review & editing, Supervision, Methodology, Conceptualization.

Declaration of competing interest

The authors declare the following financial interests/personal relationships which may be considered as potential competing interests:Josipa Bosnjak reports financial support was provided by German Research Foundation. If there are other authors, they declare that they have no known competing financial interests or personal relationships that could have appeared to influence the work reported in this paper.

Acknowledgements

The authors would like to acknowledge the support received from the fire department of the Material Testing Institute (MPA), University of Stuttgart, Germany, for there laboratory support and German Research Foundation (DFG Grant No. BO 4810/1-1), Germany for funding this project.

Data availability

Data will be made available on request.

References

[1] A. Das, J. Bošnjak, A. Sharma, Post-fire bond behaviour of reinforcement in concrete considering different bonded lengths and position of rebars, Eng. Struct. 296 (2023) 116908, https://doi.org/10.1016/j.engstruct.2023.116908.
[2] J. Bošnjak, A. Das, A. Sharma, Influence of concrete cover and transverse reinforcement on residual post-fire bond performance of reinforcement in concrete, Eng. Struct. 314 (2024) 118191, https://doi.org/10.1016/j.engstruct.2024.118191.
[3] A. Das, J. Bošnjak, A. Sharma, Investigations on the effects of rebar diameter on the post-fire bond capacity of RC flexural members and development of a novel post-fire bond model, Dev. Built Environ. 20 (2024) 100536, https://doi.org/10.1016/j.dibe.2024.100536.
[4] A. Das, A. Sharma, J. Bošnjak, Experimental and numerical investigations on the residual bond capacity of RC flexural members exposed to fire considering twin rebars, Dev. Built Environ. 20 (2024) 100551, https://doi.org/10.1016/j.dibe.2024.100551.
[5] A. Das, J. Bošnjak, A. Sharma, Numerical investigations on post fire bond behaviour of reinforcement in concrete, RILEM Tech. Lett. 4 (2019) 1–8, https://doi.org/10.21809/rilemtechlett.2019.88.
[6] J. Bošnjak, A. Sharma, K. Grauf, Mechanical properties of concrete with steel and polypropylene fibres at elevated temperatures. Fibers - special issue: recent advancements in steel fiber reinforced concrete and its applications, Fibers 7 (2019) 9, https://doi.org/10.3390/fib7020009.
[7] EN 1992-1-2:2004, Eurocode 2: Design of Concrete Structures. Part 1-2: General Rules-Structural Fire Design, European Committee for Standardization, 2004.
[8] ASTM E2748 - 12a, Standard Guide for Fire-Resistance Experiments (2017).
[9] ACI 216.1-14(19, Code Requirements for Determining Fire Resistance of Concrete and Masonry Construction Assemblies, American Concrete Institute, 2014.
[10] A. Rehman, A. Masood, S. Akhtar, S.M. Ibrahim, M. Shariq, Experimental and numerical investigation into flexural bond strength of RC beams exposed to elevated temperature, Constr. Build. Mater. 282 (2021) 122630, https://doi.org/10.1016/j.conbuildmat.2021.122630.
[11] M. Irheem, O. Elnawawy, Behaviour of rc beams with tension lap splices exposed to fire: experimental study, Int. J. Civ. Eng. Technol. 9 (2018) 1595–1612. https://www.researchgate.net/publication/328294084.
[12] M. Hossain-Zada, S. Kolagar, M. Fakoor, A. Vahedi, M. Nematzadeh, M.M.R. Tabari, Post-heating flexural behaviour of reinforced concrete beam with lap spliced bar and feasibility of improving flexural performance by adding hybrid fibers, Structures 55 (2023) 965–982, https://doi.org/10.1016/j.istruc.2023.06.082.
[13] A. Sharma, J. Bošnjak, M. Tonidis, Post-fire performance of RC beams with critical lap splices – experimental investigation and numerical validation, J. Build. Eng. 34 (2021) 102045, https://doi.org/10.1016/j.jobe.2020.102045.
[14] M. Tonidis, J. Bošnjak, A. Sharma, Post-fire performance of RC beams with critical lap splices – numerical parametric study, J. Build. Eng. 44 (2021) 102637, https://doi.org/10.1016/j.jobe.2021.102637.
[15] fib Model Code for Concrete Structures 2020, fédération internationale du béton, ISBN: 978-2-88394-175-5.
[16] DIN EN 206-1 Concrete, Part 1: Specification, Performance, Production and Conformity, 2001.
[17] ISO 834-1, Fire-resistance Tests - Elements of Building Construction - Part 1: General Requirements, International Organisation for Standardisation, Geneva (Switzerland), 1999.
[18] DIN EN 12390-3 Testing Hardened Concrete - Part 3: Compressive Strength of Test Specimens, seventh ed., 2009.
[19] DIN EN 12390-6, Testing Hardened Concrete - Part 6: Tensile Splitting Strength of Test Specimens Edition 09, 2010.
[20] DIN EN 12390-13 Testing Hardened Concrete - Part 13: Determination of Secant Modulus of Elasticity in Compression. Edition 06, 2014.
[21] DIN EN ISO 15630-1 Steel for the Reinforcement and Prestressing of Concrete - Test Methods - Part 1: Reinforcing Bars, Rods and Wire, 2019.
[22] DIN EN ISO 15630-2 Steel for the Reinforcement and Prestressing of Concrete - Test Methods - Part 2: Welded Fabric and Lattice Girders.
[23] DIN 4223:2014-12: Application of prefabricated reinforced components of autoclaved aerated concrete.
[24] J. Ožbolt, I. Kožar, R. Eligehausen, G. Periškić, Instationäres 3D Thermo mechanisches Modell für Beton (Transient 3D thermo-mechanical model for concrete), Beton- Stahlbetonbau 100 (2005) 39–51, https://doi.org/10.1002/best.200590006.
[25] J. Ožbolt, Y. Li, I. Kožar, Microplane model for concrete with relaxed kinematic constraint, Int. J. Solid Struct. 38 (2001) 2683–2711, https://doi.org/10.1016/S0020-7683(00)00177-3.
[26] G. Muciaccia, A. Consiglio, Local bond properties of reinforcement in concrete subjected to elevated temperatures: effects of clear cover, bonded length and heating and loading procedures, Eng. Struct. 230 (2021) 111594, https://doi.org/10.1016/j.engstruct.2020.111594.
[27] A. Sharma, J. Bošnjak, S. Bessert, Experimental investigations on residual bond performance in concrete subjected to elevated temperature, Eng. Struct. 187 (2019) 384–395.